ELSEVIER

Engineering Analysis with Boundary Elements 30 (2006) 176–193

ENGINEERING ANALYSIS *with* BOUNDARY ELEMENTS

www.elsevier.com/locate/enganabound

3D elastic wave propagation modelling in the presence of 2D fluid-filled thin inclusions

António Tadeu *, Paulo Amado Mendes, Julieta António

Department of Civil Engineering, University of Coimbra, Pólo II, Pinhal de Marrocos, 3030-290 Coimbra, Portugal

Received 17 January 2005; received in revised form 6 June 2005; accepted 22 August 2005

Abstract

In this paper, the traction boundary element method (TBEM) and the boundary element method (BEM), formulated in the frequency domain, are combined so as to evaluate the 3D scattered wave field generated by 2D fluid-filled thin inclusions. This model overcomes the thin-body difficulty posed when the classical BEM is applied. The inclusion may exhibit arbitrary geometry and orientation, and may have null thickness. The singular and hypersingular integrals that appear during the model's implementation are computed analytically, which overcomes one of the drawbacks of this formulation. Different source types such as plane, cylindrical and spherical sources, may excite the medium. The results provided by the proposed model are verified against responses provided by analytical models derived for a cylindrical circular fluid-filled borehole.

The performance of the proposed model is illustrated by solving the cases of a flat fluid-filled fracture with small thickness and a fluid-filled S-shaped inclusion, modelled with both small and null thickness, all of which are buried in an unbounded elastic medium. Time and frequency responses are presented when spherical pulses with a Ricker wavelet time evolution strikes the cracked medium. To avoid the aliasing phenomena in the time domain, complex frequencies are used. The effect of these complex frequencies is removed by rescaling the time responses obtained by first applying an inverse Fourier transformation to the frequency domain computations. The numerical results are analysed and a selection of snapshots from different computer animations is given. This makes it possible to understand the time evolution of the wave propagation around and through the fluid-filled inclusion.

Keywords: Wave propagation; Elastic scattering; Fluid-filled thin inclusions; Boundary element method; Traction boundary element method; 2.5D problem

1. Introduction

It is essential to fully understand how waves propagate from the source to the receiver if the signals recorded during seismic testing can themselves be understood. The relative contribution of the many wave propagation modes that may be excited by the source determines the complexity of the wave patterns recorded at the receivers. This contribution depends on the distance from the source to the receiver, the dominant frequency of the pulse, the material characteristics of the geologic formation, the type of source and the presence of fractures (cracks) [1–3]. Cracks are very important in several fields, such as determining the integrity of construction elements (in many engineering applications), and detecting and defining delamination in slabs and pavements using non-destructive evaluation techniques [4–8].

Various numerical methods have been used to study wave scattering by inclusions and thin heterogeneities, since analytical solutions are only known for simple problems [9,10]. The finite difference method (FDM) [11–16], the finite element method (FEM) [17–19], the boundary integral approach [20], the boundary element method (BEM) [21,22] and hybrid methods [23–25] are some of the techniques most often used.

In an unbounded medium the BEM is particularly efficient since it automatically satisfies the far field conditions, it can easily handle irregular geometries and only requires the discretization of the material interfaces, which is an advantage over other numerical techniques such as the FDM and the FEM. However, the BEM degenerates when thin or even null-thickness inclusions occur.

Pointer et al. [7] proposed an indirect boundary element formulation to simulate the seismic wave field scattered from an arbitrary number of fractures that are either empty or contain

* Corresponding author. Tel.: +351 239 797201; fax: +351 239 797190.
E-mail address: tadeu@dec.uc.pt (A. Tadeu).

0955-7997/$ - see front matter © 2005 Elsevier Ltd. All rights reserved.
doi:10.1016/j.enganabound.2005.08.014

elastic or fluid material. The traction boundary integral equation method is a different technique that handles the thin-body difficulty [26–29]. The appearance of hypersingular integrals is one of the difficulties posed by these formulations. Different attempts have been made to overcome this difficulty [30–33]. The traction boundary element method (TBEM) was used by Prosper [34] and Prosper and Kausel [35] to model the scattering of waves by flat and horizontal empty cracks of zero thickness in elastic media. An indirect approach was proposed for the analytical evaluation of integrals with hypersingular kernels for plane-strain cases in the 2D problem.

Most of the work published refers to the cases of 2D and, in some cases, 3D geometries and where the crack is assumed to be empty (free stress field). In real life, the crack may be either empty or it may be filled with fluid or elastic material, which determines a distinct dynamic behaviour.

This work solves the case of a crack whose geometry does not change along one direction (2D) while the source exhibits a 3D nature. This geometry is commonly referred to as a two-and-a-half-dimensional problem (2-1/2D). The solution is obtained after applying a spatial Fourier transform along the direction in which the geometry remains constant. This procedure allows the 3D solution to be computed as a summation of 2D solutions for different spatial wavenumbers. Furthermore, the crack is assumed to be filled with fluid, which determines the continuity of normal displacements and normal tractions, and null tangential stresses along the boundary of the crack. The crack may have a small or even null thickness.

The problem is solved using a mixed formulation involving the application of both the TBEM and the BEM: one of the formulations is used for the upper surface of the crack while the other models its lower surface. As noted above, the use of the TBEM leads to the integration of hypersingular kernels. In the work described in this paper, these hypersingular kernels are evaluated analytically using an indirect approach, which is accomplished by defining the dynamic equilibrium of semi-cylinders above the boundary elements, discretizing the crack. It represents an extension of the work by Prosper and Kausel [35], when they defined the behaviour of a 2D dimensional flat and horizontal crack. The combination of the displacement BEM and the traction BEM is commonly referred to as the 'Dual Boundary Element Method' [36–38].

In this paper, the 3D problem is defined and its solution described, and the boundary element formulations (BEM, TBEM and TBEM + BEM) are presented. Then the numerical solutions are verified against analytical solutions known for the case of a cylindrical circular fluid-filled borehole. The procedure for finding time signatures is outlined. The paper ends with an illustration of the applicability of the proposed technique to simulate the 3D wave propagation in the vicinity of fluid-filled thin inclusions.

2. Problem formulation

An unbounded homogeneous isotropic elastic medium, with no intrinsic attenuation, hosts a 2D fluid–filled inclusion. The hosting medium has density ρ and allows shear wave and compressional wave velocities of β and α, respectively. A Cartesian coordinate system is used with the z-axis being aligned along the direction in which the geometry of the inclusion remains constant. The inclusion is assumed to be filled with an inviscid fluid with density ρ_f, where the compressional waves propagate with a velocity of α_f. A dilatational point source, placed in the host medium at position (x_s, y_s, z_s) and oscillating with frequency ω, emits an incident field that can be expressed by the dilatational potential ϕ,

$$\phi_{\text{inc}} = \frac{A e^{i(\omega/\alpha)(\alpha t - \sqrt{(x-x_s)^2+(y-y_s)^2+(z-z_s)^2})}}{\sqrt{(x-x_s)^2+(y-y_s)^2+(z-z_s)^2}}, \tag{1}$$

where the subscript inc represents the direct incident field, A the wave amplitude and $i = \sqrt{-1}$.

In the problems where the geometry remains constant along one direction, the 3D solution may be computed after applying a Fourier transformation along that direction. Thus the 3D solution is expressed as an integration of 2D problems. This integration becomes discrete if a set of virtual sources is placed at equal distances apart along the z direction [39]. Each of these 2D problems is solved for a specific wavenumber $k_\alpha = \sqrt{(\omega^2/\alpha^2) - k_{zm}^2}$, with $\text{Im}(k_\alpha) < 0$, where $k_{zm} = (2\pi/L_{vs})m$, $(m = 0,1,\ldots,M)$, is the axial (in the z direction) wavenumber, and L_{vs} is the distance between virtual point sources equally spaced along z. The incident field is expressed at (x, y) by

$$\hat{\phi}_{\text{inc}}(\omega, x, y, k_z) = \frac{-iA}{2} H_0(k_\alpha \sqrt{(x-x_s)^2 + (y-y_s)^2}), \tag{2}$$

in which $H_n(\ldots)$ are second Hankel functions of order n. The distance L_{vs} must be sufficiently large to prevent the virtual sources from contributing to the response. It should be noted that $k_z = 0$ corresponds to the pure 2D case.

3. Different boundary integral formulations

3.1. Boundary element formulation (BEM formulation)

Considering a homogeneous elastic medium of infinite extent, containing a fluid-filled inclusion bounded by a surface S, and subjected to spatially sinusoidal harmonic line loads placed in the host solid medium at $\mathbf{x}_s$, with spatial wavenumber k_z, the boundary integral equations can be constructed by applying the reciprocity theorem, leading to:

– along the boundary, in the exterior domain (elastic medium)

$$c_{ij} u_i(\mathbf{x}_0, \omega) = \int_S t_1(\mathbf{x}, n_n, \omega) G_{i1}(\mathbf{x}, \mathbf{x}_0, \omega) \mathrm{d}s - \int_S u_j(\mathbf{x}, \omega) H_{ij}(\mathbf{x}, n_n, \mathbf{x}_0, \omega) \mathrm{d}s + u_i^{\text{inc}}(\mathbf{x}_s, \mathbf{x}_0, \omega), \tag{3}$$

– along the boundary, in the interior domain (fluid medium)

$$c_f p(\mathbf{x}_0,\omega) = \int_S q(\mathbf{x},n_n,\omega)G_f(\mathbf{x},\mathbf{x}_0,\omega)\mathrm{d}s - \int_S p(\mathbf{x},\omega)H_f(\mathbf{x},n_n,\mathbf{x}_0,\omega)\mathrm{d}s. \quad (4)$$

In Eq. (3), i, $j=1$, 2 stand for the normal and tangential directions relative to the inclusion surface, respectively, while $i, j=3$ refer to the z direction. $H_{ij}(\mathbf{x}, n_n, \mathbf{x}_0, \omega)$ are the tractions in direction j at $\mathbf{x}$ (on the boundary S) due to a unit point force in direction i at $\mathbf{x}_0$ (the collocation point), while $G_{i1}(\mathbf{x}, \mathbf{x}_0, \omega)$ are the displacements (Green's functions) in the normal direction at $\mathbf{x}$ (on the boundary S) due to a unit point force in the direction i at $\mathbf{x}_0$ (the collocation point). $u_j(\mathbf{x}, \omega)$ are the displacements in direction j at $\mathbf{x}$, while $t_1(\mathbf{x}, n_n, \omega)$ are the tractions in the normal direction at $\mathbf{x}$. $u_i^{\mathrm{inc}}(\mathbf{x}_s,\mathbf{x}_0,\omega)$ is the displacement incident field at $\mathbf{x}_0$ along direction i. The coefficient c_{ij} is equal to $\delta_{ij}/2$, where δ_{ij} is the Kronecker delta when the boundary is smooth. The vector $n_n=(\cos\theta_n, \sin\theta_n)$ is the unit outward normal at the boundary at $\mathbf{x}$. In Eq. (4), $G_f(\mathbf{x}, \mathbf{x}_0, \omega)$ and $H_f(\mathbf{x}, n_n, \mathbf{x}_0, \omega)$ are, respectively, the fundamental solutions (Green's functions) for the pressure $p(\mathbf{x}, \omega)$ and pressure gradient $q(\mathbf{x}, n_n, \omega)$ at $\mathbf{x}$ due to a virtual point pressure load at $\mathbf{x}_0$. The factor c_f is a constant defined by the shape of the boundary, taking the value 1/2 if $\mathbf{x}_0 \in S$ and S is smooth.

The compatibility between pressure gradients and displacements is obtained using the relation $u_1 = -(1/\rho\omega^2)(\partial p/\partial n_n)$, while the normal pressure corresponds to normal tractions. The boundary conditions applied along the solid–fluid interface prescribe continuity of normal displacements and normal tractions and null tangential stresses.

The required Green's functions for loads and displacements in the x, y and z directions, in the solid medium, are given in Tadeu and Kausel [40]. The derivatives of these Green's functions give the following tractions along the x, y and z directions, in the solid medium,

$$H_{rx} = 2\mu\left[\frac{\alpha^2}{2\beta^2}\frac{\partial G_{rx}}{\partial x} + \left(\frac{\alpha^2}{2\beta^2}-1\right)\left(\frac{\partial G_{ry}}{\partial y}+\frac{\partial G_{rz}}{\partial z}\right)\right]\cos\theta_n + \mu\left[\frac{\partial G_{ry}}{\partial x}+\frac{\partial G_{rx}}{\partial y}\right]\sin\theta_n$$

$$H_{ry} = 2\mu\left[\left(\frac{\alpha^2}{2\beta^2}-1\right)\left(\frac{\partial G_{rx}}{\partial x}+\frac{\partial G_{rz}}{\partial z}\right) + \frac{\alpha^2}{2\beta^2}\frac{\partial G_{ry}}{\partial y}\right]\sin\theta_n + \mu\left[\frac{\partial G_{ry}}{\partial x}+\frac{\partial G_{rx}}{\partial y}\right]\cos\theta_n \quad (5)$$

$$H_{rz} = \mu\left[\frac{\partial G_{rx}}{\partial z}+\frac{\partial G_{rz}}{\partial x}\right]\cos\theta_n + \mu\left[\frac{\partial G_{ry}}{\partial z}+\frac{\partial G_{rz}}{\partial y}\right]\sin\theta_n,$$

with $H_{rt}=H_{rt}(\mathbf{x}, n_n, \mathbf{x}_0, \omega)$, $G_{rt}=G_{rt}(\mathbf{x}, \mathbf{x}_0, \omega)$ and $r, t=x, y, z$. These expressions can be combined to obtain $H_{ij}(\mathbf{x}, n_n, \mathbf{x}_0, \omega)$ in the normal and tangential directions. In these equations $\mu=\rho\beta^2$.

The required 2-1/2D Green's functions for pressure and pressure gradients in Cartesian co-ordinates are those for an unbounded fluid medium,

$$G_f(\mathbf{x}, \mathbf{x}_0, \omega) = \frac{\mathrm{i}}{4}\mathrm{H}_0(k_{\alpha f}r)$$

$$H_f(\mathbf{x}, n_n, \mathbf{x}_0, \omega) = \frac{-\mathrm{i}}{4}k_{\alpha f}\mathrm{H}_1(k_{\alpha f}r)\frac{\partial r}{\partial n_n}, \quad (6)$$

in which $k_{\alpha f} = \sqrt{(\omega^2/\alpha_f^2)-k_z^2}$, with $\mathrm{Im}(k_{\alpha_f})<0$, and $r=\sqrt{(x-x_0)^2+(y-y_0)^2}$.

The evaluation of these integral equations for an arbitrary cross-section requires the discretization of both the boundary and boundary values. By successively applying the virtual load to each node on the boundary, a system of linear equations relating nodal tractions (and pressures) and normal displacements (and pressure gradients) is obtained, and these can be solved for the normal tractions and nodal displacements.

The required integrations are performed in closed form when the element to be integrated is the loaded element [41,42], while numerical integration, using a Gaussian quadrature scheme, applies when the element to be integrated is not the loaded one.

3.2. Traction boundary element formulation (TBEM formulation)

The BEM formulation described above degenerates in the presence of a thin fluid-filled inclusion. To overcome this difficulty the traction boundary element method (TBEM) can be formulated [34,35], leading to the following equations:

– along the boundary, in the exterior domain (elastic medium)

$$c_{i1}t_1(\mathbf{x}_0, n_n, \omega) + a_{i1}u_i(\mathbf{x}_0, \omega) = \int_S t_1(\mathbf{x}, n_n, \omega)\bar{G}_{i1}(\mathbf{x}, n_n, \mathbf{x}_0, \omega)\mathrm{d}s - \int_S u_j(\mathbf{x}, \omega)\bar{H}_{ij}(\mathbf{x}, n_n, \mathbf{x}_0, \omega)\mathrm{d}s + \bar{u}_i^{\mathrm{inc}}(\mathbf{x}_s, \mathbf{x}_0, n_n, \omega), \quad (7)$$

– along the boundary, in the interior domain (fluid medium)

$$a_f p(\mathbf{x}_0, \omega) + c_f q(\mathbf{x}_0, n_n, \omega) = \int_S q(\mathbf{x}, n_n, \omega)\bar{G}_f(\mathbf{x}, n_n, \mathbf{x}_0, \omega)\mathrm{d}s - \int_S p(\mathbf{x}, \omega)\bar{H}_f(\mathbf{x}, n_n, \mathbf{x}_0, \omega)\mathrm{d}s. \quad (8)$$

In Eq. (7), i, $j=1$, 2 stand for the normal and tangential directions relative to the inclusion surface, respectively, and i, $j=3$ refer to the z direction. These equations can be seen as resulting from the application of dipoles (dynamic doublets). As noted by Guiggiani [43] the coefficients a_{i1} and a_f are zero

for piecewise straight boundary elements and c_{i1} is equal to 1/2, when the boundary is smooth and $i=1$, and c_f is a constant defined as above. $\bar{G}_{i1}(\mathbf{x}, n_n, \mathbf{x}_0, \omega)$ and $\bar{H}_{ij}(\mathbf{x}, n_n, \mathbf{x}_0, \omega)$ are defined after the application of the traction operator to $G_{i1}(\mathbf{x}, \mathbf{x}_0, \omega)$ and $H_{ij}(\mathbf{x}, n_n, \mathbf{x}_0, \omega)$. This can be seen as the combination of the derivatives of Eq. (3), in order to x, y and z, so as to obtain stresses $\bar{G}_{i1}(\mathbf{x}, n_n, \mathbf{x}_0, \omega)$ and $\bar{H}_{ij}(\mathbf{x}, n_n, \mathbf{x}_0, \omega)$. Along the boundary element, at $\mathbf{x}$, where the unit outward normal is defined by $n_n=(\cos\theta_n, \sin\theta_n)$, and after the equilibrium of stresses, the following equations are expressed for x, y and z generated by loads also applied along x, y and z directions:

$$\bar{G}_{xr} = 2\mu\left[\frac{\alpha^2}{2\beta^2}\frac{\partial G_{xr}}{\partial x} + \left(\frac{\alpha^2}{2\beta^2}-1\right)\left(\frac{\partial G_{yr}}{\partial y}+\frac{\partial G_{zr}}{\partial z}\right)\right]\cos\theta_0 + \mu\left[\frac{\partial G_{yr}}{\partial x}+\frac{\partial G_{xr}}{\partial y}\right]\sin\theta_0$$

$$\bar{G}_{yr} = 2\mu\left[\left(\frac{\alpha^2}{2\beta^2}-1\right)\left(\frac{\partial G_{xr}}{\partial x}+\frac{\partial G_{zr}}{\partial z}\right) + \frac{\alpha^2}{2\beta^2}\frac{\partial G_{yr}}{\partial y}\right]\sin\theta_0 + \mu\left[\frac{\partial G_{yr}}{\partial x}+\frac{\partial G_{xr}}{\partial y}\right]\cos\theta_0$$

$$\bar{G}_{zr} = \mu\left[\frac{\partial G_{xr}}{\partial z}+\frac{\partial G_{zr}}{\partial x}\right]\cos\theta_0 + \mu\left[\frac{\partial G_{yr}}{\partial z}+\frac{\partial G_{zr}}{\partial y}\right]\sin\theta_0 \tag{9}$$

and

$$\bar{H}_{xr} = 2\mu\left[\frac{\alpha^2}{2\beta^2}\frac{\partial H_{xr}}{\partial x} + \left(\frac{\alpha^2}{2\beta^2}-1\right)\left(\frac{\partial H_{yr}}{\partial y}+\frac{\partial H_{zr}}{\partial z}\right)\right]\cos\theta_0 + \mu\left[\frac{\partial H_{yr}}{\partial x}+\frac{\partial H_{xr}}{\partial y}\right]\sin\theta_0$$

$$\bar{H}_{yr} = 2\mu\left[\left(\frac{\alpha^2}{2\beta^2}-1\right)\left(\frac{\partial H_{xr}}{\partial x}+\frac{\partial H_{zr}}{\partial z}\right) + \frac{\alpha^2}{2\beta^2}\frac{\partial H_{yr}}{\partial y}\right]\sin\theta_0 + \mu\left[\frac{\partial H_{yr}}{\partial x}+\frac{\partial H_{xr}}{\partial y}\right]\cos\theta_0$$

$$\bar{H}_{zr} = \mu\left[\frac{\partial H_{xr}}{\partial z}+\frac{\partial H_{zr}}{\partial x}\right]\cos\theta_0 + \mu\left[\frac{\partial H_{yr}}{\partial z}+\frac{\partial H_{zr}}{\partial y}\right]\sin\theta_0, \tag{10}$$

with $n_0=(\cos\theta_0, \sin\theta_0)$ defining the unit outward normal at $\mathbf{x}_0$ (the collocation point), $\bar{G}_{tr}=\bar{G}_{tr}(\mathbf{x}, n_n, \mathbf{x}_0, \omega)$, $G_{tr}=G_{tr}(\mathbf{x}, \mathbf{x}_0, \omega)$, $\bar{H}_{tr}=\bar{H}_{tr}(\mathbf{x}, n_n, \mathbf{x}_0, \omega)$, $H_{tr}=H_{tr}(\mathbf{x}, n_n, \mathbf{x}_0, \omega)$ and r, $t=x, y, z$.

As for $\bar{G}_{tr}$ and $\bar{H}_{tr}$, the incident field component (stresses) is obtained by analogous expressions:

$$\bar{u}_x^{\text{inc}} = 2\mu\left[\frac{\alpha^2}{2\beta^2}\frac{\partial u_x^{\text{inc}}}{\partial x} + \left(\frac{\alpha^2}{2\beta^2}-1\right)\left(\frac{\partial u_y^{\text{inc}}}{\partial y}+\frac{\partial u_z^{\text{inc}}}{\partial z}\right)\right]\cos\theta_0 + \mu\left[\frac{\partial u_y^{\text{inc}}}{\partial x}+\frac{\partial u_x^{\text{inc}}}{\partial y}\right]\sin\theta_0$$

$$\bar{u}_y^{\text{inc}} = 2\mu\left[\left(\frac{\alpha^2}{2\beta^2}-1\right)\left(\frac{\partial u_x^{\text{inc}}}{\partial x}+\frac{\partial u_z^{\text{inc}}}{\partial z}\right) + \frac{\alpha^2}{2\beta^2}\frac{\partial u_y^{\text{inc}}}{\partial y}\right]\sin\theta_0 + \mu\left[\frac{\partial u_y^{\text{inc}}}{\partial x}+\frac{\partial u_x^{\text{inc}}}{\partial y}\right]\cos\theta_0 \tag{11}$$

$$\bar{u}_z^{\text{inc}} = \mu\left[\frac{\partial u_x^{\text{inc}}}{\partial z}+\frac{\partial u_z^{\text{inc}}}{\partial x}\right]\cos\theta_0 + \mu\left[\frac{\partial u_y^{\text{inc}}}{\partial z}+\frac{\partial u_z^{\text{inc}}}{\partial y}\right]\sin\theta_0,$$

with $\bar{u}_r^{\text{inc}}=\bar{u}_r^{\text{inc}}(\mathbf{x}_s, \mathbf{x}_0, n_n, \omega)$, $u_r^{\text{inc}}=u_r^{\text{inc}}(\mathbf{x}_s, \mathbf{x}_0, \omega)$, and $r=x, y, z$.

The previous expressions can be combined so as to obtain $\bar{G}_{i1}(\mathbf{x}, n_n, \mathbf{x}_0, \omega)$, $\bar{H}_{ij}(\mathbf{x}, n_n, \mathbf{x}_0, \omega)$ and $\bar{u}_i^{\text{inc}}(\mathbf{x}_s, \mathbf{x}_0, n_n, \omega)$, in the normal and tangential directions.

The required 2-1/2D Green's functions in the fluid medium are now defined as:

$$\bar{G}_f(\mathbf{x}, n_n, \mathbf{x}_0, \omega) = \frac{i}{4}k_{\alpha f}H_1(k_{\alpha f}r)\left(\frac{\partial r}{\partial x}\frac{\partial x}{\partial n_0}+\frac{\partial r}{\partial y}\frac{\partial y}{\partial n_0}\right)$$

$$\begin{aligned}\bar{H}_f(\mathbf{x}, n_n, \mathbf{x}_0, \omega) &= \frac{i}{4}k_{\alpha f}\left\{-k_{\alpha f}H_2(k_{\alpha f}r)\left[\left(\frac{\partial r}{\partial x}\right)^2\frac{\partial x}{\partial n_n}+\frac{\partial r}{\partial x}\frac{\partial r}{\partial y}\frac{\partial y}{\partial n_n}\right] + \frac{H_1(k_{\alpha f}r)}{r}\left[\frac{\partial x}{\partial n_n}\right]\right\}\frac{\partial x}{\partial n_0} \\ &+ \frac{i}{4}k_{\alpha f}\left\{-k_{\alpha f}H_2(k_{\alpha f}r)\left[\frac{\partial r}{\partial x}\frac{\partial r}{\partial y}\frac{\partial x}{\partial n_n}+\left(\frac{\partial r}{\partial y}\right)^2\frac{\partial y}{\partial n_n}\right] + \frac{H_1(k_{\alpha f}r)}{r}\left[\frac{\partial y}{\partial n_n}\right]\right\}\frac{\partial y}{\partial n_0}.\end{aligned} \tag{12}$$

The solutions of these Eqs. (7) and (8) are defined, as before, by discretizing the boundary into N straight constant boundary elements with the collocation points located at the center of the elements. This leads to a set of integrations, which are performed using a Gaussian quadrature scheme when the element to be integrated is not the loaded element. When the element to be integrated is the loaded one, hypersingular integrals are defined, which are evaluated through an indirect approach described below.

Since the final system of equations is established assuming the normal, tangential and z directions in relation to the boundary element, the integrations along the loaded element are independent of its orientation. The integrations can therefore be performed for a horizontal boundary element, for which $\cos\theta_n=\cos\theta_0=0$ and $\sin\theta_n=\sin\theta_0=1.0$. These integrations are obtained using an indirect approach, which consists of defining the dynamic equilibrium of an isolated semi-cylinder defined above the boundary of each boundary element. Their derivation can be found in the Appendix A.

3.3. Dual BEM (TBEM+BEM) formulation

The two formulations can be combined so as to solve the above problems, and the case of a thin fluid-filled inclusion. Part of the boundary surface is loaded with monopole loads

(BEM), while the remaining part is loaded with dipoles (TBEM), which is known as the Dual BEM formulation.

When the thin fluid-filled inclusion has a fluid layer thickness tending to zero, the solution requires the implementation of a modified formulation, assuming a thin inclusion that is able to guarantee continuity of normal displacements and normal tractions, but where there are no tangential stresses.

In this case, the system of equations to solve the problem is built writing Eqs. (3) and (7) along the boundary of the thin inclusion, in the elastic medium, and the following settings ascribed: the normal displacements on the two surfaces of the inclusion are equal; the tractions on the two surfaces of the inclusion are opposite but have the same amplitude; and the tangential tractions are zero.

4. Verification of the BEM formulations

The boundary element formulations already presented, are verified through comparison with known analytical solutions. Consider a circular fluid-filled cylindrical inclusion, placed in a homogeneous elastic medium and subjected to a point dilatational load placed in this solid medium. The solution of this problem can be defined in a circular cylindrical coordinate system (r, θ, z) and evaluated in closed form using the separation of variables method [9,44].

The host elastic medium is unbounded and homogeneous, and exhibits a mass density of 2140 kg/m^3, a dilatational wave speed of 2696.5 m/s and a shear wave speed of 1451.7 m/s. The fluid filling the inclusion, with density $\rho_f = 1000$ kg/m^3, exhibits a pressure wave velocity $\alpha_f = 1500$ m/s. The point harmonic load is located at O (0.0, −0.125, 0.0 m) and two receivers are placed at R_1 (0.0, −0.075, 0.0 m) and R_2 (−0.025, 0.0, 0.0 m), as shown in Fig. 1.

The x-, y- and z-components of displacements and the pressure response have been evaluated for both receivers in the frequency range from 2000 to 64000 Hz, for an axial wavenumber $k_z = 25$ rad/m. The numerical responses in terms of displacements in the x, y and z directions, obtained by the three boundary element formulations (BEM, TBEM and TBEM+BEM, also referred to as the Dual BEM), are compared with the analytical results in Fig. 2. In the Dual BEM model, the upper half part is modelled using monopole loads (BEM solution) while the lower half part is discretized using dipole loads (TBEM solution). The plots give the real and imaginary parts of the responses, with the analytical solutions being represented by solid and dashed lines, respectively, while the marked points correspond to the three different BEM results. The numerical responses, in terms of displacement amplitudes and pressure amplitude, show a very close agreement with the analytical results, for receivers R_1 and R_2.

5. Time responses

Solutions in the time domain are obtained after the responses in the frequency domain have been computed. Time signatures are calculated by simulating a source with a

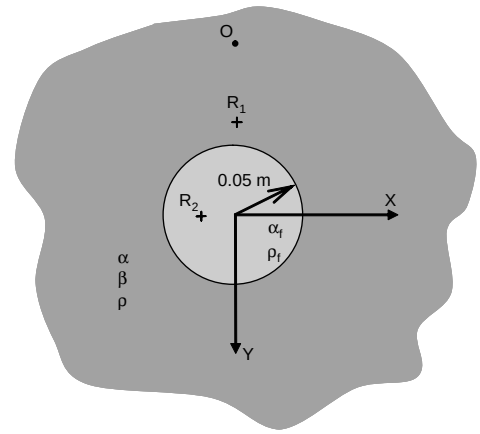

Fig. 1. Circular cylindrical fluid-filled inclusion in an unbounded elastic medium: geometry, source (O) and receivers' (R_1 and R_2) positions.

time evolution given by a Ricker pulse. This pulse decays rapidly in the time and frequency domains, and has the advantages of requiring less computational effort and easily permitting the interpretation of the time signals. The time-dependent excitation is expressed as

$$u(\tau) = A(1-2\tau^2)\mathrm{e}^{-\tau^2}, \tag{13}$$

where A is the amplitude, $\tau = (t - t_s)/t_o$, t refers to time, t_s is the time at which the maximum occurs, while πt_0 is the characteristic period of the wavelet. Its Fourier transform is given by:

$$U(\omega) = A[2\sqrt{\pi}t_o\mathrm{e}^{-\mathrm{i}\omega t_s}]\Omega^2\mathrm{e}^{-\Omega^2}, \tag{14}$$

in which $\Omega = \omega t_o/2$.

Complex frequencies with a small imaginary part of the form $\omega_c = \omega - \mathrm{i}\eta$ are used to avoid the aliasing phenomena and to minimize the contribution of the periodic virtual sources. $\eta = 0.7\ \Delta\omega$ (with $\Delta\omega$ being the increment of frequency) was chosen as the imaginary part of the angular frequency, to attenuate the wraparound by a factor of $\mathrm{e}^{0.7\Delta\omega T} = 81$, i.e. 38 dB (with $T = 1/\Delta\omega$ being the time window). This value of η is commonly used in wave propagation analysis. The use of a larger value would introduce loss of accuracy in the response, and it should not be much smaller because the aim is to achieve a maximum reduction in the contribution of the aliasing phenomena [45]. In the time domain, this procedure is taken into account by applying an exponential window $\mathrm{e}^{\eta t}$ to the response.

6. Numerical applications

Three different 2D inclusions, namely a flat fluid-filled fracture with small thickness and a fluid-filled S-shaped inclusion, modelled as having small and null thickness, and placed in a uniform elastic unbounded medium, are presented below to illustrate the capabilities of the proposed formulations.

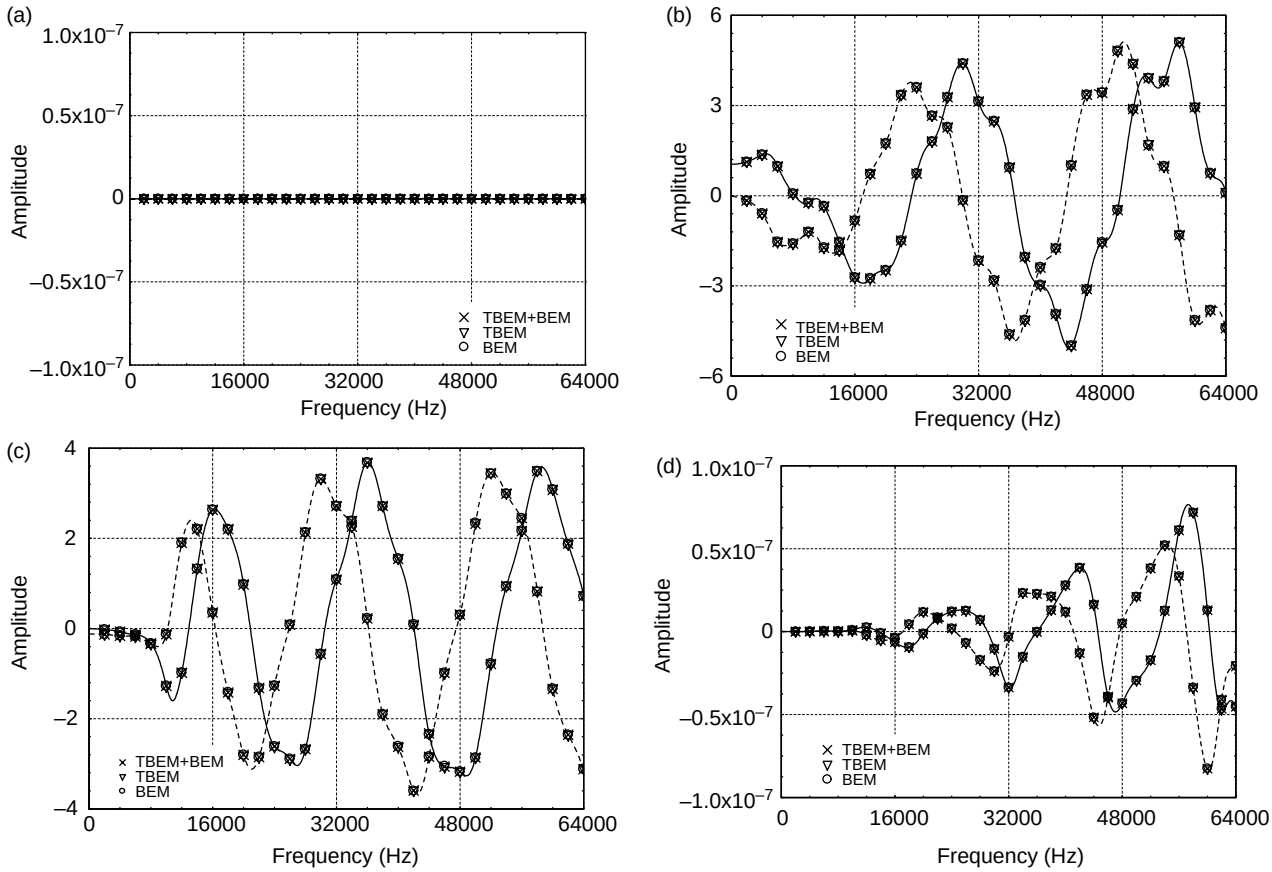

Fig. 2. Analytical vs. BEM algorithms: results for a circular cylindrical fluid-filled inclusion excited by a 2-1/2D dilatational load with $k_z = 25$ rad/m: (a) receiver R_1, x-component displacement; (b) receiver R_1, y-component displacement; (c) receiver R_1, z-component displacement; (d) receiver R_2, pressure responses.

The host elastic medium is the same for all calculations. It permits a dilatational wave velocity of 2696.5 m/s and a shear wave velocity of 1451.7 m/s. In the fluid-filled inclusions, the fluid enables a wave propagation velocity of 1500 m/s. The 3D dilatational point load excites the elastic media, placed at point O (0.0, 0.0 m), as in Figs. 3, 5 and 7.

The simulations were computed by the Dual BEM model, with the upper part of the inclusion's surface being discretized by the TBEM formulation and the lower part by the BEM formulation. An appropriate number of boundary elements was selected, defined at each frequency by the relation between the wavelength (λ)and the length of the boundary elements (L), and set at 10. All results were obtained by performing the computations in the frequency domain, in the range (2000, 256000 Hz), and time responses were determined after applying an inverse Fourier transformation with the source time evolution modelled by a Ricker pulse with a characteristic frequency of 75,000 Hz. A time window of 0.5 ms is determined by a frequency increment of 2000 Hz.

6.1. Fluid-filled 5 mm thick horizontal inclusion

The first example simulates a fluid-filled thin inclusion which is 5 mm thick. It is a horizontal heterogeneity with its extremities being modeled as semi-circumferences, as shown in Fig. 3. The minimum number of boundary elements used was 240, at 2000 Hz, 40 of which were used in the discretization of the two extremities.

Time responses were evaluated in three grids of receivers placed in the host medium along three orthogonal planes: $x = -0.15$ m, $y = 0.25$ m and $z = 0$ m (see Fig. 4). The receivers are evenly spaced at 0.003 m along the x and y directions and 0.005 m along the z direction.

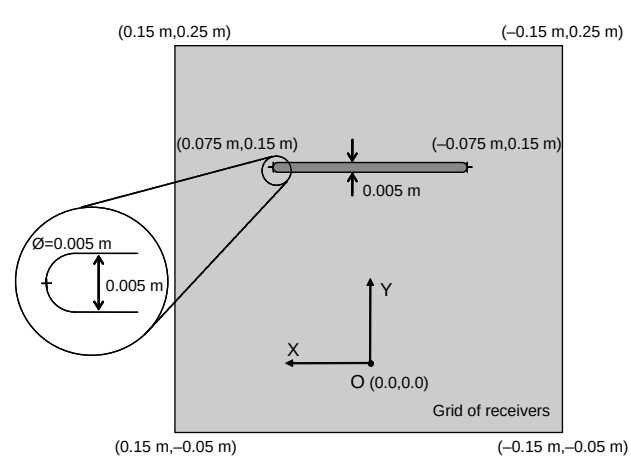

Fig. 3. Fluid-filled 5 mm thick horizontal inclusion: geometry and source and receivers' positions at xy plane.

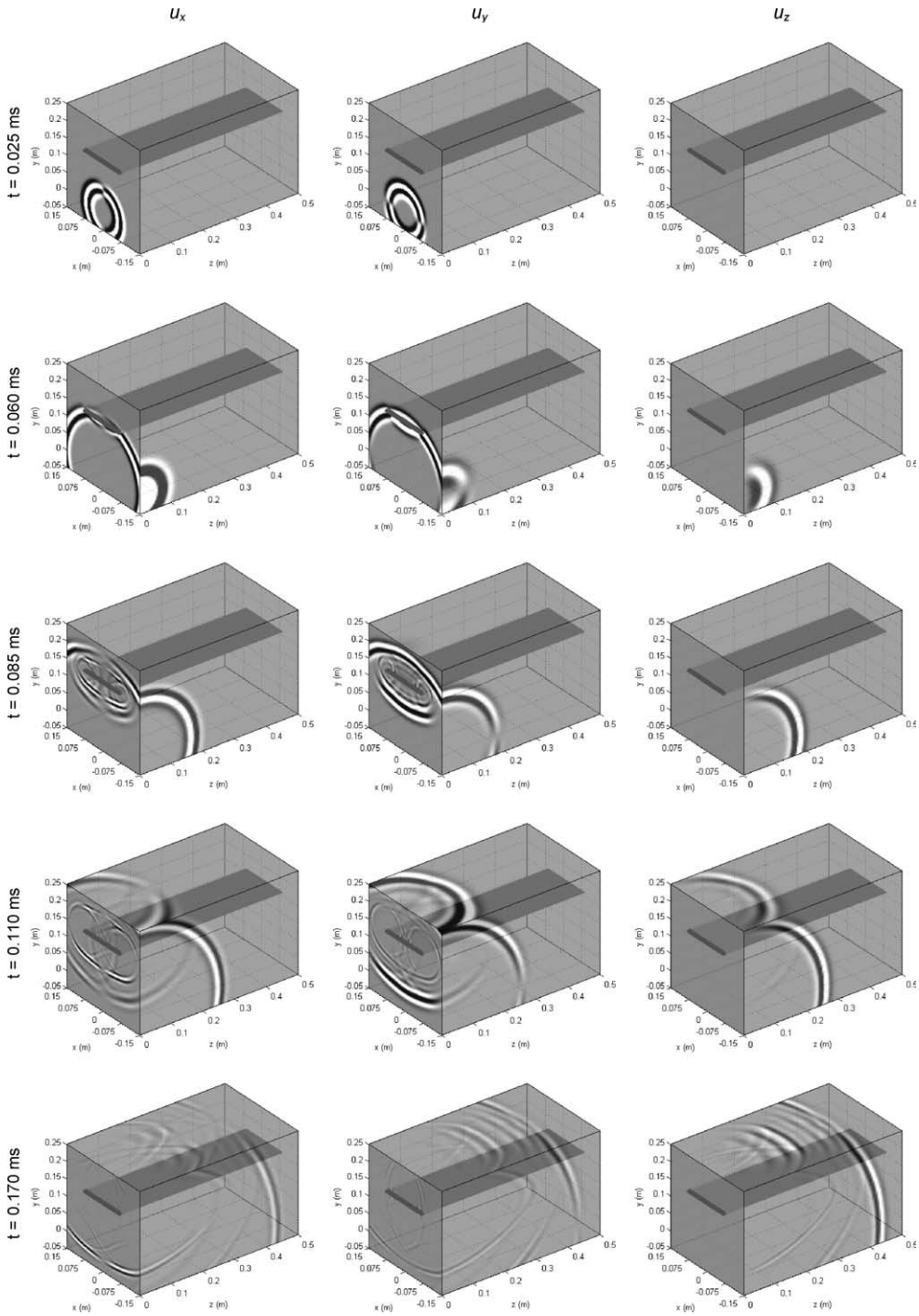

Fig. 4. Elastic scattering by a fluid-filled 5 mm thick horizontal inclusion in an unbounded medium: x-component, u_x, y-component, u_y, and z-component, u_z, displacements at different time instants.

The numerical results obtained for the wave propagation in the vicinity and through the inclusion are presented by time sequential 3D snapshots of displacements in the x, y and z directions (Fig. 4). The small thickness of the inclusion allowed the pressure responses to be calculated in the receivers placed inside the inclusion, but they are not displayed in that figure. Thus, only the displacements in the host elastic medium, which correspond to the scattering around the inclusion, are plotted in Fig. 4. This displacement field corresponds to the incident field produced by the 3D point source plus the scattered field generated by the thin inclusion in the unbounded medium. A gray scale is used, with the lighter and darker shades corresponding respectively to higher and lower displacement amplitude values.

At $t = 0.025$ ms, the waves excited by the dilatational source can be observed propagating in the elastic medium but they have not reached the fluid-filled inclusion. x- and y-component displacements are observed in the vertical plane at $z = 0$ m. The z-component is null, as that is the plane of the point source (in fact, it is a plane of symmetry). When

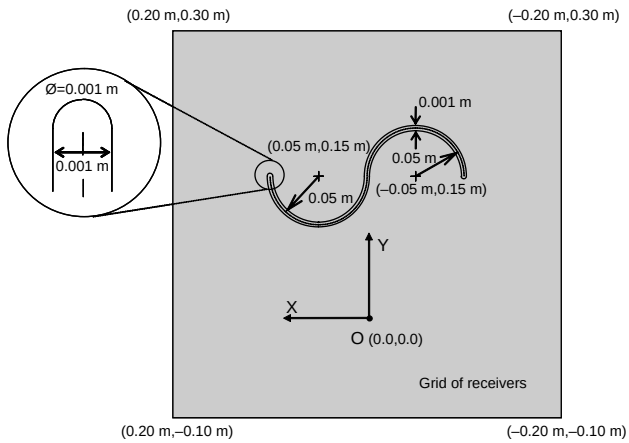

Fig. 5. Fluid-filled 1 mm thick S-shaped inclusion: geometry and source and receivers' positions at *xy* plane.

the incident pulses hit the inclusion, they are partly reflected back as P- and S-waves, and some propagate into the fluid medium as P-waves. These waves generate multiple reflections on the inclusion's upper and lower surfaces. Whenever these waves reach the inclusion's surface, they are reflected back as P-waves in fluid, and simultaneously P- and S-waves are generated that propagate away from the inclusion in the elastic medium. Besides these body waves, guided waves are generated, thus verifying the boundary conditions. At time $t=0.060$ ms, the waves have just hit the inclusion and the first reflections on its lower surface are just becoming visible. The P-waves that pass through the fluid (u_x and u_y) are in their initial development stages in the elastic medium as P- and S-waves and only denote an amplitude attenuation and a time delay in relation to the direct incident field. For all displacement components, the propagation of the incident pulse along the z direction also starts to be visible at this time instant on plane $x=-0.15$ m.

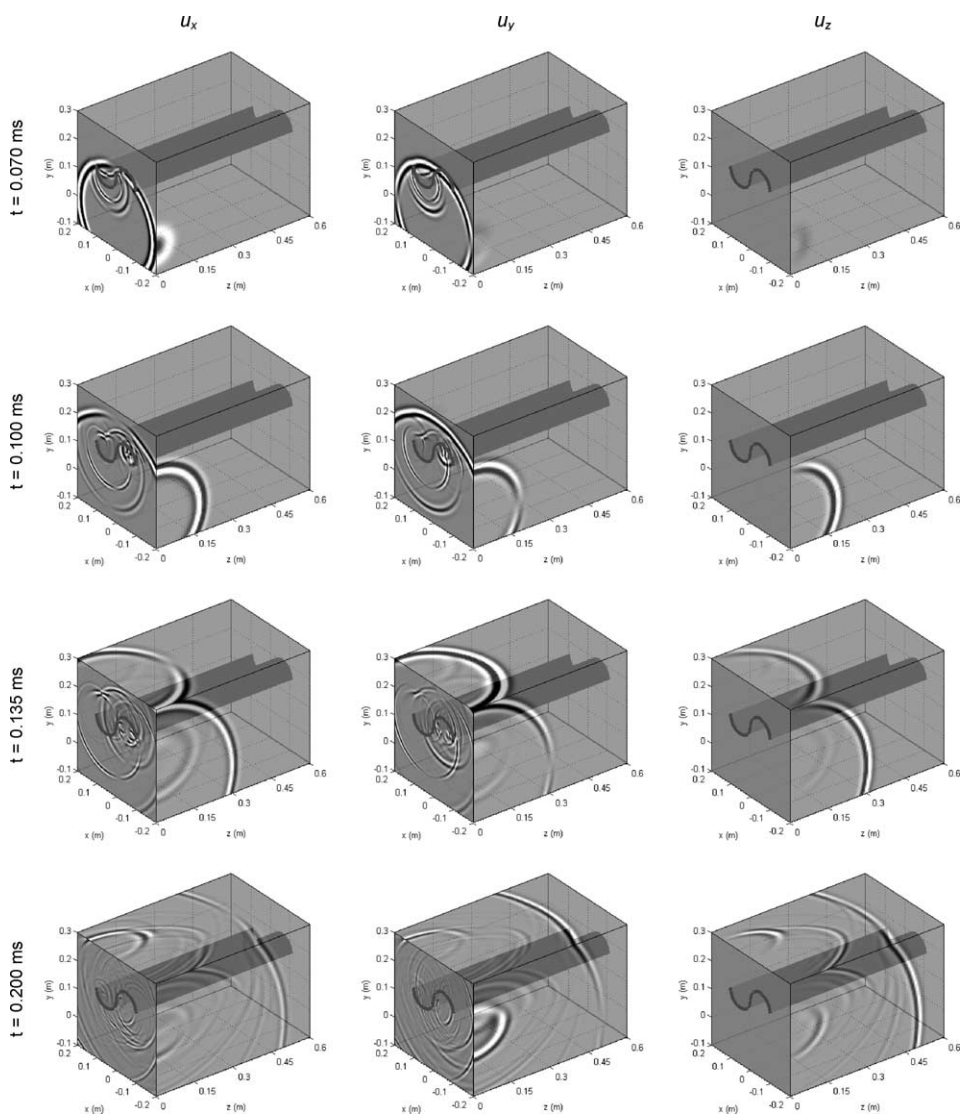

Fig. 6. Elastic scattering by a fluid-filled 1 mm thick S-shaped inclusion in an unbounded medium. *x*-component, u_x, *y*-component, u_y, and *z*-component, u_z, displacements at different time instants.

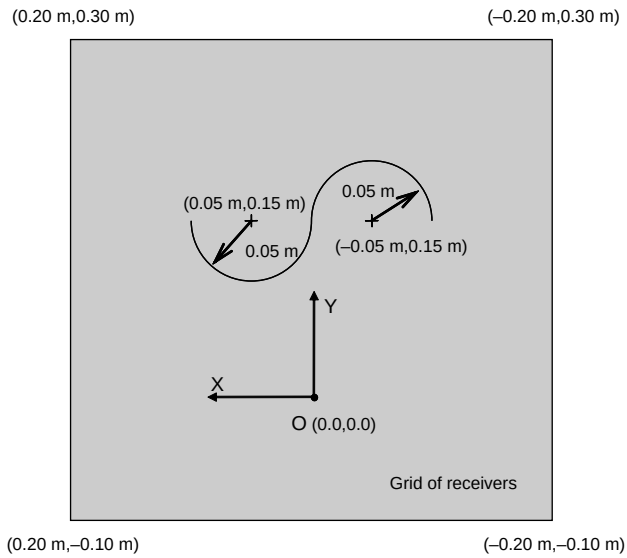

Fig. 7. Null-thickness fluid-filled S-shaped inclusion: geometry and source and receivers' positions at *xy* plane.

In the third and fourth sets of snapshots ($t=0.085$ and 0.110 ms), the reflected (as P- and S-waves) and diffracted waves on the inclusion's surface are well developed. The pulses that passed through the fluid medium have already reached the horizontal plane at $y=0.25$ m at $t=0.110$ ms. At later instants ($t=0.170$ ms), the reflected waves continue propagating through the unbounded medium, and a wave pattern caused by the multiple reflections on both the upper and lower parts of the thin element is observed in the upper grid of receivers (plane $y=0.25$ m) as it propagates along the z direction. These results clearly illustrate the 3D behavior of the wave scattering in the neighborhood of the fluid-filled heterogeneity.

6.2. Fluid-filled 1 mm thick S-shaped inclusion

The second example models the time evolution of the wave scattered by an S-shaped thin inclusion which is 1 mm thick. This thickness is maintained along the length of the inclusion, whose extremities are represented by 1 mm diameter semi-circumferences (see Fig. 5 for general geometry definition and zoom on the extremities). For the first frequency evaluated, 340 boundary elements discretized the entire boundary of the thin fluid-filled inclusion.

The x-, y- and z-components of the displacements around the inclusion are displayed in Fig. 6, after computation at the grids of receivers corresponding to planes $x=-0.20$ m, $y=0.30$ m and $z=0$ m. The 3D perspectives shown in this figure display the total displacement fields in the host elastic medium at different time instants from $t=0.070$ to 0.200 ms. The same gray scale described above is adopted in these plots.

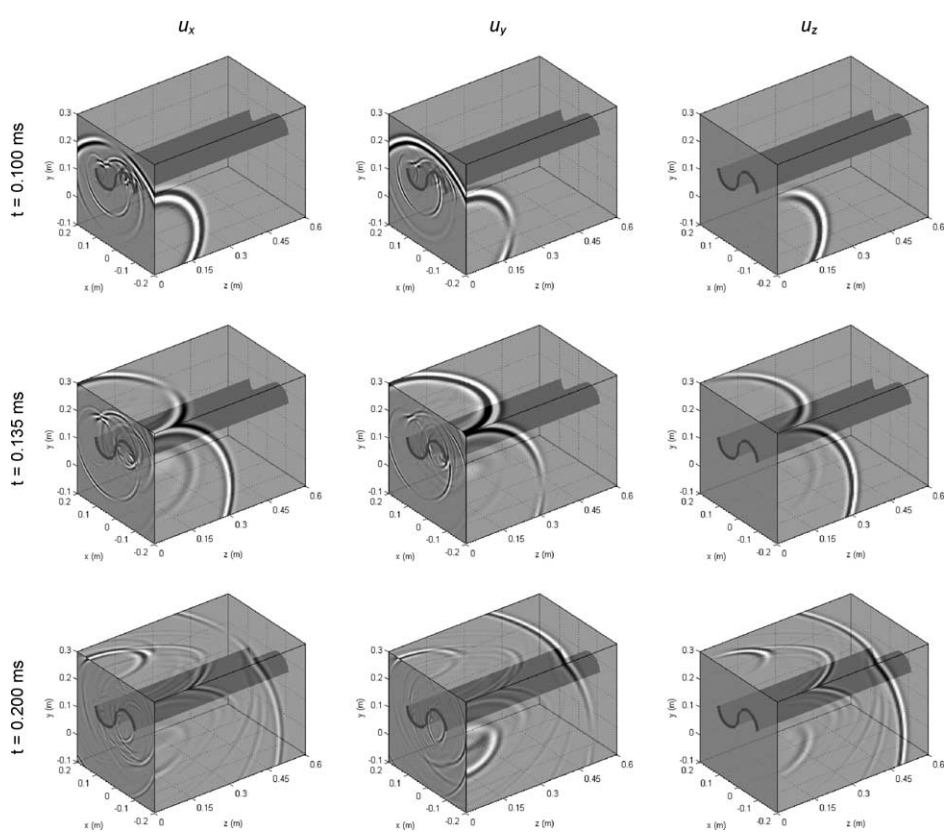

Fig. 8. Elastic scattering by a null-thickness fluid-filled S-shaped inclusion in an unbounded medium. x-component, u_x, y-component, u_y, and z-component, u_z, displacements at different time instants.

At the initial time instants, since the incident wave field is the same as in the previous example, a very similar behavior of the waves excited by the 3D source is obtained (but not presented in Fig. 6). However, the wave scattering becomes more complex after reaching the S-shaped thin inclusion. As the incident waves reach the fluid-filled inclusion, they are reflected as P- and S-waves and transmitted to the opposite side of the inclusion after passing through the fluid medium as P-waves. In relation to the undisturbed incident wave field, amplitude attenuation is observed but the time delay for the wave front is less significant than in the previous case. Multiple wave reflections inside the thin inclusion still exhibit a similar behavior to that already described for the horizontal inclusion. The geometry of the S-shaped heterogeneity causes the reflected energy to remain trapped at the concave part facing the source point, and generates a complex wave field pattern which is most evident at $t=0.135$ and 0.200 ms.

Note that this method is able to correctly describe the stress singularity at the tips of the thin inclusion assuming that the crack keeps its geometry in the presence of wave propagation. If this method were applied to the definition of the crack growth, as required in fracture mechanics, it would need to be modified.

6.3. Null-thickness fluid-filled S-shaped inclusion

The last numerical example corresponds to a problem whose geometry is similar to the previous case; however, the thickness of the inclusion tends to zero. It is a very thin fluid-filled inclusion, which has been modelled by implementing a TBEM+BEM formulation, which, for a null-thickness inclusion, prescribes null tangential stresses along its boundary. The surface being discretized is loaded with the TBEM and the BEM formulations in its upper and lower parts, respectively, and these are, in fact, defined by coincident lines. The geometry of the problem and the source point location are outlined in Fig. 7.

Some plots, corresponding to different time instants in the simulation of the wave propagation after the source starts emitting at $t=0.0$ ms, are shown in Fig. 8. The wave field pattern observed is very similar to the previous numerical example. However, the wave amplitude attenuation and the wave front time delay are not perceptible, since the inclusion has no thickness. For the same reason, there are no multiple reflections inside the previous inclusions, so the transmitted wave field is simpler. It is also visible that the amplitude of the P-waves being reflected back by the null-thickness inclusion is smaller than that amplitude registered in the previous 1 mm thick case. The reflected waves still concentrate at the concave part of the heterogeneity facing the source point, where they generate a complex wave field pattern most evident at plane $z=0$ m.

7. Conclusions

This paper has proposed different boundary element formulations for studying wave propagation in the vicinity of thin, or even null-thickness, fluid-filled inclusions, since the classical direct boundary element method (BEM) fails in these situations. A traction boundary element formulation (TBEM) and a mixed formulation that combines the BEM and the TBEM (known as the Dual BEM formulation) were successfully verified against known analytical solutions for the case of fluid-filled circular cylindrical inclusions, and they also compare very well with the BEM results for those cases. To overcome the problems that arise when applying the TBEM and the TBEM+BEM formulations, which lead to integrals with hypersingular kernels, an indirect approach for performing those integrations analytically is suggested.

Two-and-a-half-dimensional problems are addressed in this work, where 3D solutions are computed by summing 2D solutions for different spatial wavenumbers, after applying a spatial Fourier transformation along the direction in which the geometry of the problem does not change. This procedure allows the computation of the 3D solution without having to discretize the domain along the third dimension (the z direction). This represents a substantial decrease in computational costs, in terms of both computer storage memory and CPU effort.

The results for the different numerical applications presented here demonstrate that the proposed methodology is able to evaluate the scattered fields in the presence of thin fluid-filled inclusions embedded in unbounded homogeneous elastic media. The results correspond to the inclusions' various geometries, namely, to a thin horizontal inclusion 5 mm thick and to two S-shaped inclusions, one a 1 mm thick inclusion and the other an inclusion whose thickness tends to zero. The presence of the fluid filling the inclusions changes the undisturbed wave pattern in an unbounded medium considerably, demonstrating the interaction between the solid and the fluid media.

Appendix A. Hypersingular integrations

A.1. Hypersingular integrations resulting from Eq. (7), applied in the exterior domain (elastic medium)

Along a horizontal element, the normal, tangential and z directions correspond to the y, x and z directions, respectively. Therefore, from Eq. (10),

$$\bar{H}_{xr} = \mu\left[\frac{\partial H_{yr}}{\partial x} + \frac{\partial H_{xr}}{\partial y}\right] \tag{A1}$$

$$\bar{H}_{yr} = 2\mu\left[\left(\frac{\alpha^2}{2\beta^2}-1\right)\left(\frac{\partial H_{xr}}{\partial x} + \frac{\partial H_{zr}}{\partial z}\right) + \frac{\alpha^2}{2\beta^2}\frac{\partial H_{yr}}{\partial y}\right] \tag{A2}$$

$$\bar{H}_{zr} = \mu\left[\frac{\partial H_{yr}}{\partial z} + \frac{\partial H_{zr}}{\partial y}\right]. \tag{A3}$$

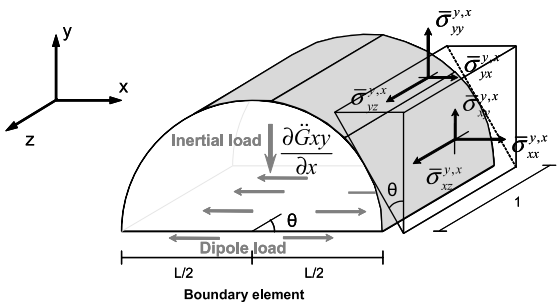

Fig. 9. Dynamic equilibrium of a semi-cylinder defined above the boundary element for the integration of $\partial H_{xx}/\partial x$, $\partial H_{xy}/\partial x$ and $\partial H_{xz}/\partial x$.

The indirect approach used to evaluate the hypersingular integrals corresponds to the dynamic equilibrium of an isolated semi-cylinder defined above the boundary element as illustrated in Figs. 9–15.

A.1.1. Load along the normal direction

The resultants along the horizontal, vertical and z directions are given by:

$$\bar{H}_{yx} = 2\mu\left[\left(\frac{\alpha^2}{2\beta^2}-1\right)\left(\frac{\partial H_{xx}}{\partial x}+\frac{\partial H_{zx}}{\partial z}\right) + \frac{\alpha^2}{2\beta^2}\frac{\partial H_{yx}}{\partial y}\right] \quad \text{(horizontal resultant)} \tag{A4}$$

$$\bar{H}_{yy} = 2\mu\left[\left(\frac{\alpha^2}{2\beta^2}-1\right)\left(\frac{\partial H_{xy}}{\partial x}+\frac{\partial H_{zy}}{\partial z}\right) + \frac{\alpha^2}{2\beta^2}\frac{\partial H_{yy}}{\partial y}\right] \quad \text{(vertical resultant)} \tag{A5}$$

$$\bar{H}_{yz} = 2\mu\left[\left(\frac{\alpha^2}{2\beta^2}-1\right)\left(\frac{\partial H_{xz}}{\partial x}+\frac{\partial H_{zz}}{\partial z}\right) + \frac{\alpha^2}{2\beta^2}\frac{\partial H_{yz}}{\partial y}\right] \quad (z \text{ resultant}) \tag{A6}$$

The definition of the terms $\partial H_{xx}/\partial x$, $\partial H_{xy}/\partial x$ and $\partial H_{xz}/\partial x$ can be written as:

$$\frac{\partial H_{xx}}{\partial x} = \bar{\sigma}_{xx}^{y,x}\cos\theta + \bar{\sigma}_{yx}^{y,x}\sin\theta \tag{A7}$$

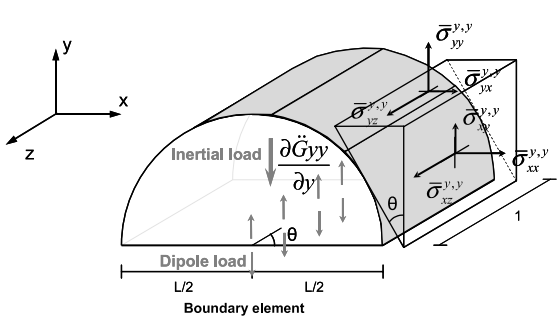

Fig. 10. Dynamic equilibrium of a semi-cylinder defined above the boundary element for the integration of $\partial H_{yx}/\partial y$, $\partial H_{yy}/\partial y$ and $\partial H_{yz}/\partial y$.

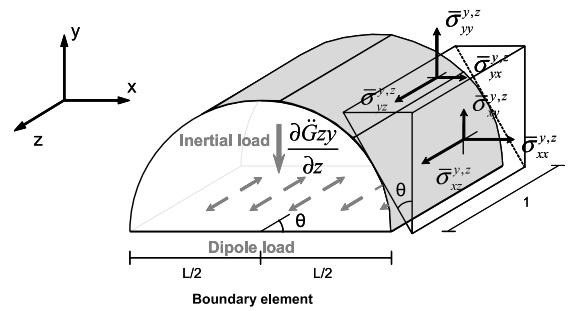

Fig. 11. Dynamic equilibrium of a semi-cylinder defined above the boundary element for the integration of $\partial H_{zx}/\partial z$, $\partial H_{zy}/\partial z$ and $\partial H_{zz}/\partial z$.

$$\frac{\partial H_{xy}}{\partial x} = \bar{\sigma}_{yy}^{y,x}\sin\theta + \bar{\sigma}_{xy}^{y,x}\cos\theta$$

$$\frac{\partial H_{xz}}{\partial x} = \bar{\sigma}_{xz}^{y,x}\cos\theta + \bar{\sigma}_{yz}^{y,x}\sin\theta,$$

with

$$\bar{\sigma}_{xx}^{y,x} = 2\mu\left[\frac{\alpha^2}{2\beta^2}\frac{\partial^2 G_{xx}}{\partial x\partial x} + \left(\frac{\alpha^2}{2\beta^2}-1\right)\left(\frac{\partial^2 G_{xy}}{\partial x\partial y}+\frac{\partial^2 G_{xz}}{\partial x\partial z}\right)\right],$$

$$\bar{\sigma}_{yx}^{y,x} = \mu\left[\frac{\partial^2 G_{xy}}{\partial x\partial x}+\frac{\partial^2 G_{xx}}{\partial x\partial y}\right],$$

$$\bar{\sigma}_{yy}^{y,x} = 2\mu\left[\left(\frac{\alpha^2}{2\beta^2}-1\right)\left(\frac{\partial^2 G_{xx}}{\partial x\partial x}+\frac{\partial^2 G_{xz}}{\partial x\partial z}\right) + \frac{\alpha^2}{2\beta^2}\frac{\partial^2 G_{xy}}{\partial x\partial y}\right],$$

$$\bar{\sigma}_{xy}^{y,x} = \mu\left[\frac{\partial^2 G_{xy}}{\partial x\partial x}+\frac{\partial^2 G_{xx}}{\partial x\partial y}\right],$$

$$\bar{\sigma}_{xz}^{y,x} = \mu\left[\frac{\partial^2 G_{xx}}{\partial x\partial z}+\frac{\partial^2 G_{xz}}{\partial x\partial x}\right],$$

$$\bar{\sigma}_{yz}^{y,x} = \mu\left[\frac{\partial^2 G_{xy}}{\partial x\partial z}+\frac{\partial^2 G_{xz}}{\partial x\partial y}\right],$$

and can be seen as the application of a dipole load and an inertial load defined as shown in Fig. 9.

The dynamic equilibrium of this semi-cylinder in Fig. 9 (with volume V) is determined by computing the resulting components of the forces defined along the surface of the cylinder S_{sc} and of the inertial load in the volume defined by the

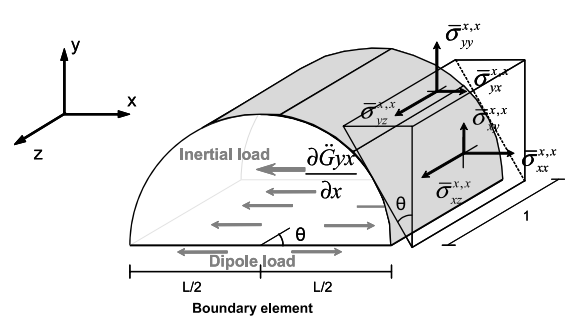

Fig. 12. Dynamic equilibrium of a semi-cylinder defined above the boundary element for the integration of $\partial H_{yx}/\partial x$, $\partial H_{yy}/\partial x$ and $\partial H_{yz}/\partial x$.

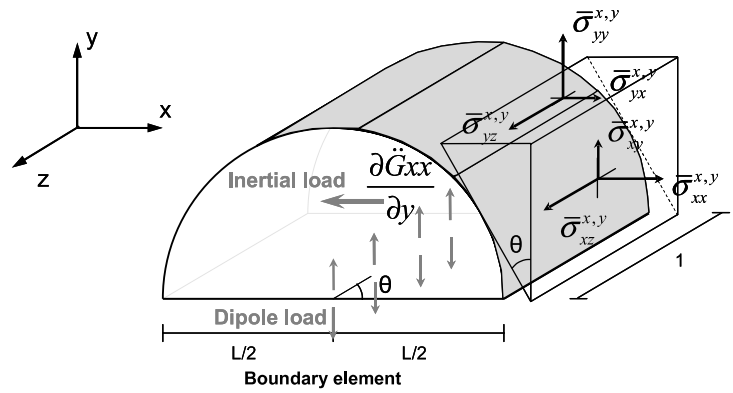

Fig. 13. Dynamic equilibrium of a semi-cylinder defined above the boundary element for the integration of $\partial H_{xx}/\partial y$, $\partial H_{xy}/\partial y$ and $\partial H_{xz}/\partial y$.

boundary element S_{BE} and the surface of the cylinder S_{sc}:

$$\begin{aligned}\int_{S_{\mathrm{BE}}} \frac{\partial H_{xx}}{\partial x}\mathrm{d}S_{\mathrm{BE}} &= \int_{S_{\mathrm{SC}}} (\bar{\sigma}_{xx}^{y,x}\cos\theta + \bar{\sigma}_{yx}^{y,x}\sin\theta)\mathrm{d}S_{\mathrm{SC}} \\ &= \int_0^{\pi} (\bar{\sigma}_{xx}^{y,x}\cos\theta + \bar{\sigma}_{yx}^{y,x}\sin\theta)\frac{L}{2}\mathrm{d}\theta = 0,\end{aligned} \tag{A8}$$

where L corresponds to the length of the boundary element;

$$\begin{aligned}\int_{S_{\mathrm{BE}}} \frac{\partial H_{xy}}{\partial x}\mathrm{d}S_{\mathrm{BE}} &= \int_{S_{\mathrm{SC}}} (\bar{\sigma}_{yy}^{y,x}\sin\theta + \bar{\sigma}_{xy}^{y,x}\cos\theta)\mathrm{d}S_{\mathrm{SC}} - \int_V \rho\frac{\partial \ddot{G}_{xy}}{\partial x}\mathrm{d}V \\ &= \int_0^{\pi} (\bar{\sigma}_{yy}^{y,x}\sin\theta + \bar{\sigma}_{xy}^{y,x}\cos\theta)\frac{L}{2}\mathrm{d}\theta \\ &\quad + \rho\omega^2\int_0^{\pi}\int_0^{L/2}\frac{\partial G_{xy}}{\partial x} r\mathrm{d}r\,\mathrm{d}\theta \\ &= \frac{\mathrm{i}}{2}\left[k_\alpha \mathrm{H}_1\left(k_\alpha\frac{L}{2}\right)\left(1-\frac{2\beta^2}{\alpha^2}\right)\right. \\ &\quad \left. -\frac{4}{Lk_s^2}\chi_2\left(\frac{L}{2}\right) - \frac{L}{3}\frac{k_z^2}{k_s^2}\chi_2\left(\frac{L}{2}\right)\right],\end{aligned} \tag{A9}$$

with

$k_\beta = \sqrt{\omega^2/\beta^2 - k_z^2}$,

$k_s = \omega/\beta$ and $\chi_n(L/2) = k_\beta^n \mathrm{H}_n(k_\beta(L/2)) - k_\alpha^n H_n(k_\alpha(L/2))$;

$$\begin{aligned}\int_{S_{\mathrm{BE}}} \frac{\partial H_{xz}}{\partial x}\mathrm{d}S_{\mathrm{BE}} &= \int_{S_{\mathrm{SC}}} (\bar{\sigma}_{xz}^{y,x}\cos\theta + \bar{\sigma}_{yz}^{y,x}\sin\theta)\mathrm{d}S_{\mathrm{SC}} \\ &= \int_0^{\pi} (\bar{\sigma}_{xz}^{y,x}\cos\theta + \bar{\sigma}_{yz}^{y,x}\sin\theta)\frac{L}{2}\mathrm{d}\theta \\ &= \frac{-k_z\pi L}{8k_s^2}\left[k_\beta^3\mathrm{H}_1\left(k_\beta\frac{L}{2}\right) - k_\alpha^3\mathrm{H}_1\left(k_\alpha\frac{L}{2}\right)\right. \\ &\quad \left. -\frac{1}{2}k_\beta k_s^2\mathrm{H}_1\left(k_\beta\frac{L}{2}\right)\right].\end{aligned} \tag{A10}$$

The terms $\partial H_{yx}/\partial y$, $\partial H_{yy}/\partial y$ and $\partial H_{yz}/\partial y$ are defined by:

$$\frac{\partial H_{yx}}{\partial y} = \bar{\sigma}_{xx}^{y,y}\cos\theta + \bar{\sigma}_{yx}^{y,y}\sin\theta \tag{A11}$$

$$\frac{\partial H_{yy}}{\partial y} = \bar{\sigma}_{yy}^{y,y}\sin\theta + \bar{\sigma}_{xy}^{y,y}\cos\theta$$

$$\frac{\partial H_{yz}}{\partial y} = \bar{\sigma}_{xz}^{y,y}\cos\theta + \bar{\sigma}_{yz}^{y,y}\sin\theta,$$

with

$$\bar{\sigma}_{xx}^{y,y} = 2\mu\left[\frac{\alpha^2}{2\beta^2}\frac{\partial^2 G_{yx}}{\partial y\partial x} + \left(\frac{\alpha^2}{2\beta^2}-1\right)\left(\frac{\partial^2 G_{yy}}{\partial y\partial y} + \frac{\partial^2 G_{yz}}{\partial y\partial z}\right)\right],$$

$$\bar{\sigma}_{yx}^{y,y} = \mu\left[\frac{\partial^2 G_{yy}}{\partial y\partial x} + \frac{\partial^2 G_{yx}}{\partial y\partial y}\right],$$

$$\bar{\sigma}_{yy}^{y,y} = 2\mu\left[\left(\frac{\alpha^2}{2\beta^2}-1\right)\left(\frac{\partial^2 G_{yx}}{\partial y\partial x} + \frac{\partial^2 G_{yz}}{\partial y\partial z}\right) + \frac{\alpha^2}{2\beta^2}\frac{\partial^2 G_{yy}}{\partial y\partial y}\right],$$

$$\bar{\sigma}_{xy}^{y,y} = \mu\left[\frac{\partial^2 G_{yy}}{\partial y\partial x} + \frac{\partial^2 G_{yx}}{\partial y\partial y}\right],$$

$$\bar{\sigma}_{xz}^{y,y} = \mu\left[\frac{\partial^2 G_{yx}}{\partial y\partial z} + \frac{\partial^2 G_{yz}}{\partial y\partial x}\right],$$

$$\bar{\sigma}_{yz}^{y,y} = \mu\left[\frac{\partial^2 G_{yy}}{\partial y\partial z} + \frac{\partial^2 G_{yz}}{\partial y\partial y}\right],$$

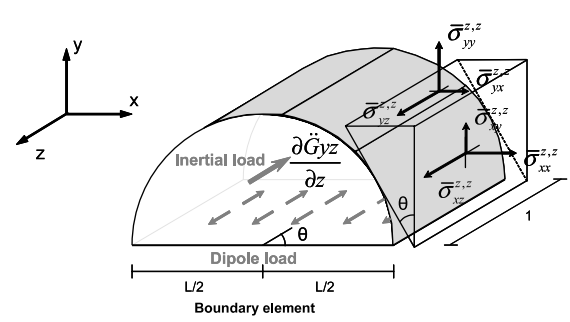

Fig. 14. Dynamic equilibrium of a semi-cylinder defined above the boundary element for the integration of $\partial H_{yx}/\partial z$, $\partial H_{yy}/\partial z$ and $\partial H_{yz}/\partial z$.

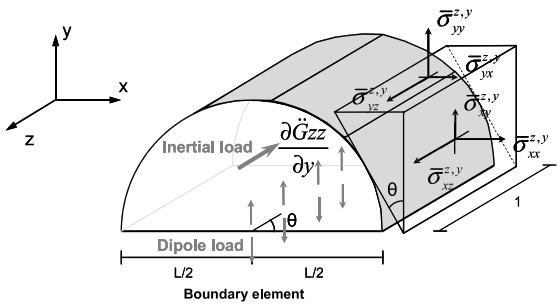

Fig. 15. Dynamic equilibrium of a semi-cylinder defined above the boundary element for the integration of $\partial H_{zx}/\partial y$, $\partial H_{zy}/\partial y$ and $\partial H_{zz}/\partial y$.

and can be taken as the application of a dipole load and an inertial load defined as in Fig. 10.

The dynamic equilibrium of this semi-cylinder in Fig. 10 (with volume V) is expressed by the computation of the resulting components of the forces acting along the surface of the cylinder S_{sc} and of the inertial load in the volume limited by the boundary element S_{BE} and the surface of the cylinder S_{sc}:

$$\begin{aligned}\int_{S_{BE}} \frac{\partial H_{yx}}{\partial y}\mathrm{d}S_{BE} &= \int_{S_{SC}} (\bar{\sigma}_{xx}^{y,y}\cos\theta + \bar{\sigma}_{yx}^{y,y}\sin\theta)\mathrm{d}S_{SC} \\ &= \int_0^{\pi} (\bar{\sigma}_{xx}^{y,y}\cos\theta + \bar{\sigma}_{yx}^{y,y}\sin\theta)\frac{L}{2}\mathrm{d}\theta = 0;\end{aligned} \tag{A12}$$

$$\begin{aligned}\int_{S_{BE}} \frac{\partial H_{yy}}{\partial y}\mathrm{d}S_{BE} &= \int_{S_{SC}} (\bar{\sigma}_{yy}^{y,y}\sin\theta + \bar{\sigma}_{xy}^{y,y}\cos\theta)\mathrm{d}S_{SC} - \int_V \rho\frac{\partial\ddot{G}_{yy}}{\partial y}\mathrm{d}V \\ &= \int_0^{\pi} (\bar{\sigma}_{yy}^{y,y}\sin\theta + \bar{\sigma}_{xy}^{y,y}\cos\theta)\frac{L}{2}\mathrm{d}\theta \\ &\quad + \rho\omega^2\int_0^{\pi}\int_0^{L/2}\frac{\partial G_{yy}}{\partial y} r\mathrm{d}r\,\mathrm{d}\theta \\ &= -\mathrm{i}\left[-\frac{1}{2}k_z^2\int_0^{L/2}\mathrm{H}_0(k_\beta r)\mathrm{d}r - \frac{1}{2}k_\alpha^2\int_0^{L/2}\mathrm{H}_0(k_\alpha r)\mathrm{d}r\right. \\ &\quad -\frac{2}{Lk_s^2}\chi_2\left(\frac{L}{2}\right) + \frac{1}{2}k_\alpha\mathrm{H}_1\left(k_\alpha\frac{L}{2}\right) \\ &\quad + \frac{L}{12k_s^2}(-k_s^2k_z^2 + 4k_z^4)\mathrm{H}_0\left(k_\beta\frac{L}{2}\right) \\ &\quad + \frac{k_\beta}{3}\frac{k_z^2}{k_s^2}\mathrm{H}_1\left(k_\beta\frac{L}{2}\right) + \frac{L}{3}\frac{k_\alpha^2k_z^2}{k_s^2}\mathrm{H}_0\left(k_\alpha\frac{L}{2}\right) \\ &\quad \left. -\frac{k_\alpha}{3}\frac{k_z^2}{k_s^2}\mathrm{H}_1\left(k_\alpha\frac{L}{2}\right)\right],\end{aligned} \tag{A13}$$

where

$$\int_0^{L/2}\mathrm{H}_0(kr)\mathrm{d}r = \frac{L}{2}\mathrm{H}_0\left(k\frac{L}{2}\right) + \pi\frac{L}{4}\left[\mathrm{H}_1\left(k\frac{L}{2}\right)\mathrm{S}_0\left(k\frac{L}{2}\right) - \mathrm{H}_0\left(k\frac{L}{2}\right)\mathrm{S}_1\left(k\frac{L}{2}\right)\right],$$

with $k=k_\alpha$ or $k=k_\beta$, and $\mathrm{S}_n(\ldots)$ are Struve functions of order n.

$$\begin{aligned}\int_{S_{BE}} \frac{\partial H_{yz}}{\partial y}\mathrm{d}S_{BE} &= \int_{S_{SC}} (\bar{\sigma}_{xz}^{y,y}\cos\theta + \bar{\sigma}_{yz}^{y,y}\sin\theta)\mathrm{d}S_{SC} \\ &= \int_0^{\pi} (\bar{\sigma}_{xz}^{y,y}\cos\theta + \bar{\sigma}_{yz}^{y,y}\sin\theta)\frac{L}{2}\mathrm{d}\theta \\ &= \frac{-k_z\pi L}{8k_s^2}\left[k_\beta^3\mathrm{H}_1\left(k_\beta\frac{L}{2}\right) - k_\alpha^3\mathrm{H}_1\left(k_\alpha\frac{L}{2}\right)\right. \\ &\quad \left. -\frac{1}{2}k_\beta k_s^2\mathrm{H}_1\left(k_\beta\frac{L}{2}\right)\right].\end{aligned} \tag{A14}$$

The definition of the derivatives $\partial H_{zx}/\partial z$, $\partial H_{zy}/\partial z$ and $\partial H_{zz}/\partial z$ can be given by:

$$\begin{aligned}\frac{\partial H_{zx}}{\partial z} &= \bar{\sigma}_{xx}^{y,z}\cos\theta + \bar{\sigma}_{yx}^{y,z}\sin\theta \\ \frac{\partial H_{zy}}{\partial z} &= \bar{\sigma}_{yy}^{y,z}\sin\theta + \bar{\sigma}_{xy}^{y,z}\cos\theta \\ \frac{\partial H_{zz}}{\partial z} &= \bar{\sigma}_{xz}^{y,z}\cos\theta + \bar{\sigma}_{yz}^{y,z}\sin\theta,\end{aligned} \tag{A15}$$

where

$$\bar{\sigma}_{xx}^{y,z} = 2\mu\left[\frac{\alpha^2}{2\beta^2}\frac{\partial^2 G_{zx}}{\partial z\partial x} + \left(\frac{\alpha^2}{2\beta^2} - 1\right)\left(\frac{\partial^2 G_{zy}}{\partial z\partial y} + \frac{\partial^2 G_{zz}}{\partial z\partial z}\right)\right],$$

$$\bar{\sigma}_{yx}^{y,z} = \mu\left[\frac{\partial^2 G_{zy}}{\partial z\partial x} + \frac{\partial^2 G_{zx}}{\partial z\partial y}\right],$$

$$\bar{\sigma}_{yy}^{y,z} = 2\mu\left[\left(\frac{\alpha^2}{2\beta^2} - 1\right)\left(\frac{\partial^2 G_{zx}}{\partial z\partial x} + \frac{\partial^2 G_{zz}}{\partial z\partial z}\right) + \frac{\alpha^2}{2\beta^2}\frac{\partial^2 G_{zy}}{\partial z\partial y}\right],$$

$$\bar{\sigma}_{xy}^{y,z} = \mu\left[\frac{\partial^2 G_{zy}}{\partial z\partial x} + \frac{\partial^2 G_{zx}}{\partial z\partial y}\right],$$

$$\bar{\sigma}_{xz}^{y,z} = \mu\left[\frac{\partial^2 G_{zx}}{\partial z\partial z} + \frac{\partial^2 G_{zz}}{\partial z\partial x}\right],$$

$$\bar{\sigma}_{yz}^{y,z} = \mu\left[\frac{\partial^2 G_{zy}}{\partial z\partial z} + \frac{\partial^2 G_{zz}}{\partial z\partial y}\right],$$

and can be interpreted as the application of a dipole load and an inertial load as described in Fig. 11.

The evaluation of the resulting components of the forces found along the surface of the cylinder S_{sc} and of the inertial

load in the volume defined by the boundary element S_{BE} and the surface of the cylinder S_{sc} expresses the dynamic equilibrium of that semi-cylinder in Fig. 11 (with volume V):

$$\int_{S_{BE}} \frac{\partial H_{zx}}{\partial z} \mathrm{d}S_{BE} = \int_{S_{SC}} (\bar{\sigma}_{xx}^{y,z} \cos\theta + \bar{\sigma}_{yx}^{y,z} \sin\theta) \mathrm{d}S_{SC} = \int_0^{\pi} (\bar{\sigma}_{xx}^{y,z} \cos\theta + \bar{\sigma}_{yx}^{y,z} \sin\theta) \frac{L}{2} \mathrm{d}\theta = 0; \quad \text{(A16)}$$

$$\begin{aligned}\int_{S_{BE}} \frac{\partial H_{zy}}{\partial z} \mathrm{d}S_{BE} &= \int_{S_{SC}} (\bar{\sigma}_{yy}^{y,z} \sin\theta + \bar{\sigma}_{xy}^{y,z} \cos\theta) \mathrm{d}S_{SC} - \int_V \rho \frac{\partial \ddot{G}_{zy}}{\partial z} \mathrm{d}V \\ &= \int_0^{\pi} (\bar{\sigma}_{yy}^{y,z} \sin\theta + \bar{\sigma}_{xy}^{y,z} \cos\theta) \frac{L}{2} \mathrm{d}\theta \\ &\quad + \rho\omega^2 \int_0^{\pi} \int_0^{L/2} \frac{\partial G_{zy}}{\partial z} r \mathrm{d}r\, \mathrm{d}\theta \\ &= \mathrm{i} \frac{L k_z^2}{4} \left[-\frac{2}{L} \int_0^{L/2} \mathrm{H}_0(k_\beta r) \mathrm{d}r + \frac{2}{L} \int_0^{L/2} \mathrm{H}_0(k_\alpha r) \mathrm{d}r \right. \\ &\quad + \frac{1}{k_p^2} \chi_2\left(\frac{L}{2}\right) + \left(\frac{1}{k_s^2} - \frac{1}{k_p^2}\right) \frac{4}{L} \chi_1\left(\frac{L}{2}\right) \\ &\quad - \mathrm{H}_0\left(k_\beta \frac{L}{2}\right) - \mathrm{H}_0\left(k_\alpha \frac{L}{2}\right) + \frac{k_\beta^2}{k_p^2} \mathrm{H}_0\left(k_\beta \frac{L}{2}\right) \\ &\quad + \frac{k_z^2}{k_p^2} \mathrm{H}_0\left(k_\alpha \frac{L}{2}\right) + 2\frac{k_z^2}{k_s^2} \mathrm{H}_0\left(k_\beta \frac{L}{2}\right) \\ &\quad \left. -2\frac{k_z^2}{k_s^2} \mathrm{H}_0\left(k_\alpha \frac{L}{2}\right) \right]; \end{aligned} \quad \text{(A17)}$$

$$\begin{aligned}\int_{S_{BE}} \frac{\partial H_{zz}}{\partial z} \mathrm{d}S_{BE} &= \int_{S_{SC}} (\bar{\sigma}_{xz}^{y,z} \cos\theta + \bar{\sigma}_{yz}^{y,z} \sin\theta) \mathrm{d}S_{SC} \\ &= \int_0^{\pi} (\bar{\sigma}_{xz}^{y,z} \cos\theta + \bar{\sigma}_{yz}^{y,z} \sin\theta) \frac{L}{2} \mathrm{d}\theta \\ &= \frac{-k_z \pi L}{8 k_s^2} \left[2k_z^2 \chi_1\left(\frac{L}{2}\right) - k_\beta k_s^2 \mathrm{H}_1\left(k_\beta \frac{L}{2}\right) \right]. \end{aligned} \quad \text{(A18)}$$

A.1.2. Load along the tangential direction

Along the horizontal, vertical and z directions, the resultants are defined by:

$$\bar{H}_{xx} = \mu \left[\frac{\partial H_{yx}}{\partial x} + \frac{\partial H_{xx}}{\partial y} \right] \quad \text{(horizontal resultant)} \quad \text{(A19)}$$

$$\bar{H}_{xy} = \mu \left[\frac{\partial H_{yy}}{\partial x} + \frac{\partial H_{xy}}{\partial y} \right] \quad \text{(vertical resultant)} \quad \text{(A20)}$$

$$\bar{H}_{xz} = \mu \left[\frac{\partial H_{yz}}{\partial x} + \frac{\partial H_{xz}}{\partial y} \right] \quad (z \text{ resultant}) \quad \text{(A21)}$$

The terms $\partial H_{yx}/\partial x$, $\partial H_{yy}/\partial x$ and $\partial H_{yz}/\partial x$ can be written as follows:

$$\begin{aligned} \frac{\partial H_{yx}}{\partial x} &= \bar{\sigma}_{xx}^{x,x} \cos\theta + \bar{\sigma}_{yx}^{x,x} \sin\theta \\ \frac{\partial H_{yy}}{\partial x} &= \bar{\sigma}_{yy}^{x,x} \sin\theta + \bar{\sigma}_{xy}^{x,x} \cos\theta \\ \frac{\partial H_{yz}}{\partial x} &= \bar{\sigma}_{xz}^{x,x} \cos\theta + \bar{\sigma}_{yz}^{x,x} \sin\theta, \end{aligned} \quad \text{(A22)}$$

with

$$\bar{\sigma}_{xx}^{x,x} = 2\mu \left[\frac{\alpha^2}{2\beta^2} \frac{\partial^2 G_{yx}}{\partial x \partial x} + \left(\frac{\alpha^2}{2\beta^2} - 1 \right) \left(\frac{\partial^2 G_{yy}}{\partial x \partial y} + \frac{\partial^2 G_{yz}}{\partial x \partial z} \right) \right],$$

$$\bar{\sigma}_{yx}^{x,x} = \mu \left[\frac{\partial^2 G_{yy}}{\partial x \partial x} + \frac{\partial^2 G_{yx}}{\partial x \partial y} \right],$$

$$\bar{\sigma}_{yy}^{x,x} = 2\mu \left[\left(\frac{\alpha^2}{2\beta^2} - 1 \right) \left(\frac{\partial^2 G_{yx}}{\partial x \partial x} + \frac{\partial^2 G_{yz}}{\partial x \partial z} \right) + \frac{\alpha^2}{2\beta^2} \frac{\partial^2 G_{yy}}{\partial x \partial y} \right],$$

$$\bar{\sigma}_{xy}^{x,x} = \mu \left[\frac{\partial^2 G_{yy}}{\partial x \partial x} + \frac{\partial^2 G_{yx}}{\partial x \partial y} \right],$$

$$\bar{\sigma}_{xz}^{x,x} = \mu \left[\frac{\partial^2 G_{yx}}{\partial x \partial z} + \frac{\partial^2 G_{yz}}{\partial x \partial x} \right],$$

$$\bar{\sigma}_{yz}^{x,x} = \mu \left[\frac{\partial^2 G_{yy}}{\partial x \partial z} + \frac{\partial^2 G_{yz}}{\partial x \partial y} \right],$$

and can be taken as the application of a dipole load and an inertial load given as in Fig. 12.

The dynamic equilibrium of this semi-cylinder in Fig. 12 (with volume V) is given by the components of the forces found along the surface of the cylinder S_{sc} and of the inertial load in the volume defined by the boundary element S_{BE} and the surface of the cylinder S_{sc}:

$$\begin{aligned}\int_{S_{BE}} \frac{\partial H_{yx}}{\partial x} \mathrm{d}S_{BE} &= \int_{S_{SC}} (\bar{\sigma}_{xx}^{x,x} \cos\theta + \bar{\sigma}_{yx}^{x,x} \sin\theta) \mathrm{d}S_{SC} - \int_V \rho \frac{\partial \ddot{G}_{yx}}{\partial x} \mathrm{d}V \\ &= \int_0^{\pi} (\bar{\sigma}_{xx}^{x,x} \cos\theta + \bar{\sigma}_{yx}^{x,x} \sin\theta) \frac{L}{2} \mathrm{d}\theta \\ &\quad + \rho\omega^2 \int_0^{\pi} \int_0^{L/2} \frac{\partial G_{yx}}{\partial x} r \mathrm{d}r\, \mathrm{d}\theta = \frac{\mathrm{i}}{2} \left[k_\beta \mathrm{H}_1\left(k_\beta \frac{L}{2}\right) \right. \\ &\quad \left. - \frac{4}{L k_s^2} \chi_2\left(\frac{L}{2}\right) - \frac{L}{3} \frac{k_z^2}{k_s^2} \chi_2(L/2) \right]; \end{aligned} \quad \text{(A23)}$$

$$\int_{S_{BE}} \frac{\partial H_{yy}}{\partial x} \mathrm{d}S_{BE} = \int_{S_{SC}} (\bar{\sigma}_{yy}^{x,x} \sin\theta + \bar{\sigma}_{xy}^{x,x} \cos\theta) \mathrm{d}S_{SC} = \int_0^{\pi} (\bar{\sigma}_{yy}^{x,x} \sin\theta + \bar{\sigma}_{xy}^{x,x} \cos\theta) \frac{L}{2} \mathrm{d}\theta = 0; \quad \text{(A24)}$$

$$\int_{S_{BE}} \frac{\partial H_{yz}}{\partial x} \mathrm{d}S_{BE} = \int_{S_{SC}} (\bar{\sigma}_{xz}^{x,x} \cos\theta + \bar{\sigma}_{yz}^{x,x} \sin\theta) \mathrm{d}S_{SC} = \int_0^{\pi} (\bar{\sigma}_{xz}^{x,x} \cos\theta + \bar{\sigma}_{yz}^{x,x} \sin\theta) \frac{L}{2} \mathrm{d}\theta = 0. \quad \text{(A25)}$$

The derivatives $\partial H_{xx}/\partial y$, $\partial H_{xy}/\partial y$ and $\partial H_{xz}/\partial y$ can be defined by:

$$\frac{\partial H_{xx}}{\partial y} = \bar{\sigma}_{xx}^{x,y} \cos\theta + \bar{\sigma}_{yx}^{x,y} \sin\theta$$

$$\frac{\partial H_{xy}}{\partial y} = \bar{\sigma}_{yy}^{x,y} \sin\theta + \bar{\sigma}_{xy}^{x,y} \cos\theta$$

$$\frac{\partial H_{xz}}{\partial y} = \bar{\sigma}_{xz}^{x,y} \cos\theta + \bar{\sigma}_{yz}^{x,y} \sin\theta, \quad \text{(A26)}$$

with

$$\bar{\sigma}_{xx}^{x,y} = 2\mu \left[\frac{\alpha^2}{2\beta^2} \frac{\partial^2 G_{xx}}{\partial y \partial x} + \left(\frac{\alpha^2}{2\beta^2} - 1 \right) \left(\frac{\partial^2 G_{xy}}{\partial y \partial y} + \frac{\partial^2 G_{xz}}{\partial y \partial z} \right) \right],$$

$$\bar{\sigma}_{yx}^{x,y} = \mu \left[\frac{\partial^2 G_{yy}}{\partial y \partial x} + \frac{\partial^2 G_{xx}}{\partial y \partial y} \right],$$

$$\bar{\sigma}_{yy}^{x,y} = 2\mu \left[\left(\frac{\alpha^2}{2\beta^2} - 1 \right) \left(\frac{\partial^2 G_{xx}}{\partial y \partial x} + \frac{\partial^2 G_{xz}}{\partial y \partial z} \right) + \frac{\alpha^2}{2\beta^2} \frac{\partial^2 G_{xy}}{\partial y \partial y} \right],$$

$$\bar{\sigma}_{xy}^{x,y} = \mu \left[\frac{\partial^2 G_{xy}}{\partial y \partial x} + \frac{\partial^2 G_{xx}}{\partial y \partial y} \right],$$

$$\bar{\sigma}_{xz}^{x,y} = \mu \left[\frac{\partial^2 G_{xx}}{\partial y \partial z} + \frac{\partial^2 G_{xz}}{\partial y \partial x} \right],$$

$$\bar{\sigma}_{yz}^{x,y} = \mu \left[\frac{\partial^2 G_{xy}}{\partial y \partial z} + \frac{\partial^2 G_{xz}}{\partial y \partial y} \right],$$

and can be deduced as the application of a dipole load and an inertial load illustrated in Fig. 13.

The dynamic equilibrium of this semi-cylinder in Fig. 13 (with volume V) is found by calculating the resulting components of the forces defined along the surface of the cylinder S_{sc} and of the inertial load in the volume defined by the boundary element S_{BE} and the surface of the cylinder S_{sc}:

$$\int_{S_{BE}} \frac{\partial H_{xx}}{\partial y} \mathrm{d}S_{BE} = \int_{S_{SC}} (\bar{\sigma}_{xx}^{x,y} \cos\theta + \bar{\sigma}_{yx}^{x,y} \sin\theta) \mathrm{d}S_{SC} - \int_V \rho \frac{\partial \ddot{G}_{xx}}{\partial y} \mathrm{d}V$$
$$= \int_0^{\pi} (\bar{\sigma}_{xx}^{x,y} \cos\theta + \bar{\sigma}_{yx}^{x,y} \sin\theta) \frac{L}{2} \mathrm{d}\theta + \rho\omega^2 \int_0^{\pi} \int_0^{L/2} \frac{\partial G_{xx}}{\partial y} r \mathrm{d}r \, \mathrm{d}\theta$$
$$= \frac{\mathrm{i}}{2} \left[k_s^2 \int_0^{L/2} \mathrm{H}_0(k_\beta r) \mathrm{d}r - \left(\frac{4}{L} + \frac{L k_z^2}{3} \right) \frac{1}{k_s^2} \chi_2 \left(\frac{L}{2} \right) - k_\beta \mathrm{H}_1 \left(k_\beta \frac{L}{2} \right) - \frac{L}{2} (k_s^2 - k_\beta^2) \mathrm{H}_0 \left(k_\beta \frac{L}{2} \right) \right]; \quad \text{(A27)}$$

$$\int_{S_{BE}} \frac{\partial H_{xy}}{\partial y} \mathrm{d}S_{BE} = \int_{S_{SC}} (\bar{\sigma}_{yy}^{x,y} \sin\theta + \bar{\sigma}_{xy}^{x,y} \cos\theta) \mathrm{d}S_{SC} = \int_0^{\pi} (\bar{\sigma}_{yy}^{x,y} \sin\theta + \bar{\sigma}_{xy}^{x,y} \cos\theta) \frac{L}{2} \mathrm{d}\theta = 0; \quad \text{(A28)}$$

$$\int_{S_{BE}} \frac{\partial H_{xz}}{\partial y} \mathrm{d}S_{BE} = \int_{S_{SC}} (\bar{\sigma}_{xz}^{x,y} \cos\theta + \bar{\sigma}_{yz}^{x,y} \sin\theta) \mathrm{d}S_{SC} = \int_0^{\pi} (\bar{\sigma}_{xz}^{x,y} \cos\theta + \bar{\sigma}_{yz}^{x,y} \sin\theta) \frac{L}{2} \mathrm{d}\theta = 0. \quad \text{(A29)}$$

A.1.3. Load along the z direction

For the present load, the resultants along the three directions (horizontal, vertical and z) can be written as:

$$\bar{H}_{zx} = \mu \left[\frac{\partial H_{yx}}{\partial z} + \frac{\partial H_{zx}}{\partial y} \right] \quad \text{(horizontal resultant)} \quad \text{(A30)}$$

$$\bar{H}_{zy} = \mu \left[\frac{\partial H_{yy}}{\partial z} + \frac{\partial H_{zy}}{\partial y} \right] \quad \text{(vertical resutant)} \quad \text{(A31)}$$

$$\bar{H}_{zz} = \mu \left[\frac{\partial H_{yz}}{\partial z} + \frac{\partial H_{zz}}{\partial y} \right] \quad (z \text{ resultant}) \quad \text{(A32)}$$

The terms $\partial H_{yx}/\partial z$, $\partial H_{yy}/\partial z$ and $\partial H_{yz}/\partial z$ can be expressed by:

$$\frac{\partial H_{yx}}{\partial z} = \bar{\sigma}_{xx}^{z,z} \cos\theta + \bar{\sigma}_{yx}^{z,z} \sin\theta \quad \text{(A33)}$$

$$\frac{\partial H_{yy}}{\partial z} = \bar{\sigma}_{yy}^{z,z} \sin\theta + \bar{\sigma}_{xy}^{z,z} \cos\theta$$

$$\frac{\partial H_{yz}}{\partial z} = \bar{\sigma}_{xz}^{z,z} \cos\theta + \bar{\sigma}_{yz}^{z,z} \sin\theta,$$

with

$$\bar{\sigma}_{xx}^{z,z} = 2\mu\left[\frac{\alpha^2}{2\beta^2}\frac{\partial^2 G_{yx}}{\partial z\partial x} + \left(\frac{\alpha^2}{2\beta^2}-1\right)\left(\frac{\partial^2 G_{yy}}{\partial z\partial y} + \frac{\partial^2 G_{yz}}{\partial z\partial z}\right)\right],$$

$$\bar{\sigma}_{yx}^{z,z} = \mu\left[\frac{\partial^2 G_{yy}}{\partial z\partial x} + \frac{\partial^2 G_{yx}}{\partial z\partial y}\right],$$

$$\bar{\sigma}_{yy}^{z,z} = 2\mu\left[\left(\frac{\alpha^2}{2\beta^2}-1\right)\left(\frac{\partial^2 G_{yx}}{\partial z\partial x} + \frac{\partial^2 G_{yz}}{\partial z\partial z}\right) + \frac{\alpha^2}{2\beta^2}\frac{\partial^2 G_{yy}}{\partial z\partial y}\right],$$

$$\bar{\sigma}_{xy}^{z,z} = \mu\left[\frac{\partial^2 G_{yy}}{\partial z\partial x} + \frac{\partial^2 G_{yx}}{\partial z\partial y}\right],$$

$$\bar{\sigma}_{xz}^{z,z} = \mu\left[\frac{\partial^2 G_{yx}}{\partial z\partial z} + \frac{\partial^2 G_{yz}}{\partial z\partial x}\right],$$

$$\bar{\sigma}_{yz}^{z,z} = \mu\left[\frac{\partial^2 G_{yy}}{\partial z\partial z} + \frac{\partial^2 G_{yz}}{\partial z\partial y}\right],$$

and can be assumed as the result of the application of a dipole load and an inertial load given in Fig. 14.

The dynamic equilibrium of this semi-cylinder in Fig. 14 (with volume V) is characterized by the evaluation of the resulting components of the existing forces along the surface of the cylinder S_{sc} and of the inertial load in the volume defined by the boundary element S_{BE} and the surface of the cylinder S_{sc}:

$$\int_{S_{BE}} \frac{\partial H_{yx}}{\partial z}\mathrm{d}S_{BE} = \int_{S_{SC}} (\bar{\sigma}_{xx}^{z,z}\cos\theta + \bar{\sigma}_{yx}^{z,z}\sin\theta)\mathrm{d}S_{SC} = \int_0^{\pi} (\bar{\sigma}_{xx}^{z,z}\cos\theta + \bar{\sigma}_{yx}^{z,z}\sin\theta)\frac{L}{2}\mathrm{d}\theta = 0; \tag{A34}$$

$$\begin{aligned}\int_{S_{BE}} \frac{\partial H_{yy}}{\partial z}\mathrm{d}S_{BE} &= \int_{S_{SC}} (\bar{\sigma}_{yy}^{z,z}\sin\theta + \bar{\sigma}_{xy}^{z,z}\cos\theta)\mathrm{d}S_{SC} \\ &= \int_0^{\pi} (\bar{\sigma}_{yy}^{z,z}\sin\theta + \bar{\sigma}_{xy}^{z,z}\cos\theta)\frac{L}{2}\mathrm{d}\theta \\ &= \frac{-k_z\pi L}{8k_s^2}\left[-k_z^2\chi_1\left(\frac{L}{2}\right) - \frac{1}{2}k_s^2 k_\beta \mathrm{H}_1\left(k_\beta\frac{L}{2}\right) - \frac{1}{2}k_s^2 k_\alpha \mathrm{H}_1\left(k_\alpha\frac{L}{2}\right)\right];\end{aligned} \tag{A35}$$

$$\begin{aligned}\int_{S_{BE}} \frac{\partial H_{yz}}{\partial z}\mathrm{d}S_{BE} &= \int_{S_{SC}} (\bar{\sigma}_{xz}^{z,z}\cos\theta + \bar{\sigma}_{yz}^{z,z}\sin\theta)\mathrm{d}S_{SC} - \int_V \rho\frac{\partial \ddot{G}_{yz}}{\partial z}\mathrm{d}V \\ &= \int_0^{\pi} (\bar{\sigma}_{xz}^{z,z}\cos\theta + \bar{\sigma}_{yz}^{z,z}\sin\theta)\frac{L}{2}\mathrm{d}\theta \\ &\quad + \rho\omega^2\int_0^{\pi}\int_0^{L/2}\frac{\partial G_{yz}}{\partial z}r\mathrm{d}r\,\mathrm{d}\theta = -\frac{\mathrm{i}k_z^2}{2}\left[\int_0^{L/2}\mathrm{H}_0(k_\beta r)\mathrm{d}r \right. \\ &\quad - \int_0^{L/2}\mathrm{H}_0(k_\alpha r)\mathrm{d}r - \frac{\mathrm{L}}{k_s^2}\chi_2\left(\frac{L}{2}\right) + \frac{2}{k_s^2}\chi_1\left(\frac{L}{2}\right) \\ &\quad \left. - L\mathrm{H}_0\left(k_\beta\frac{L}{2}\right) + \frac{L}{2}\mathrm{H}_0\left(k_\alpha\frac{L}{2}\right)\right].\end{aligned} \tag{A36}$$

The definition of the terms $\partial H_{zx}/\partial y$, $\partial H_{zy}/\partial y$ and $\partial H_{zz}/\partial y$ can be written as:

$$\frac{\partial H_{zx}}{\partial y} = \bar{\sigma}_{xx}^{z,y}\cos\theta + \bar{\sigma}_{yx}^{z,y}\sin\theta$$

$$\frac{\partial H_{zy}}{\partial y} = \bar{\sigma}_{yy}^{z,y}\sin\theta + \bar{\sigma}_{xy}^{z,y}\cos\theta$$

$$\frac{\partial H_{zz}}{\partial y} = \bar{\sigma}_{xz}^{z,y}\cos\theta + \bar{\sigma}_{yz}^{z,y}\sin\theta, \tag{A37}$$

with

$$\bar{\sigma}_{xx}^{z,y} = 2\mu\left[\frac{\alpha^2}{2\beta^2}\frac{\partial^2 G_{zx}}{\partial y\partial x} + \left(\frac{\alpha^2}{2\beta^2}-1\right)\left(\frac{\partial^2 G_{zy}}{\partial y\partial y} + \frac{\partial^2 G_{zz}}{\partial y\partial z}\right)\right],$$

$$\bar{\sigma}_{yx}^{z,y} = \mu\left[\frac{\partial^2 G_{zy}}{\partial y\partial x} + \frac{\partial^2 G_{zx}}{\partial y\partial y}\right],$$

$$\bar{\sigma}_{yy}^{z,y} = 2\mu\left[\left(\frac{\alpha^2}{2\beta^2}-1\right)\left(\frac{\partial^2 G_{zx}}{\partial y\partial x} + \frac{\partial^2 G_{zz}}{\partial y\partial z}\right) + \frac{\alpha^2}{2\beta^2}\frac{\partial^2 G_{zy}}{\partial y\partial y}\right],$$

$$\bar{\sigma}_{xz}^{z,y} = \mu\left[\frac{\partial^2 G_{zx}}{\partial y\partial z} + \frac{\partial^2 G_{zz}}{\partial y\partial x}\right],$$

$$\bar{\sigma}_{yz}^{z,y} = \mu\left[\frac{\partial^2 G_{zy}}{\partial y\partial z} + \frac{\partial^2 G_{zz}}{\partial y\partial y}\right],$$

and can be seen as the application of a dipole load and an inertial load defined as in Fig. 15.

The dynamic equilibrium of this semi-cylinder in Fig. 15 (with volume V) is defined by computing the resulting components of the forces defined along the surface of the cylinder S_{sc} and of the inertial load in the volume defined by the boundary element S_{BE} and the surface of the cylinder S_{sc}:

$$\int_{S_{\mathrm{BE}}} \frac{\partial H_{zx}}{\partial y} \mathrm{d}S_{\mathrm{BE}} = \int_{S_{\mathrm{SC}}} (\bar{\sigma}_{xx}^{z,y} \cos\theta + \bar{\sigma}_{yx}^{z,y} \sin\theta) \mathrm{d}S_{\mathrm{SC}} = \int_0^{\pi} (\bar{\sigma}_{xx}^{z,y} \cos\theta + \bar{\sigma}_{yx}^{z,y} \sin\theta) \frac{L}{2} \mathrm{d}\theta = 0; \tag{A38}$$

$$\begin{aligned}\int_{S_{\mathrm{BE}}} \frac{\partial H_{zy}}{\partial y} \mathrm{d}S_{\mathrm{BE}} &= \int_{S_{\mathrm{SC}}} (\bar{\sigma}_{yy}^{z,y} \sin\theta + \bar{\sigma}_{xy}^{z,y} \cos\theta) \mathrm{d}S_{\mathrm{SC}} \\ &= \int_0^{\pi} (\bar{\sigma}_{yy}^{z,y} \sin\theta + \bar{\sigma}_{xy}^{z,y} \cos\theta) \frac{L}{2} \mathrm{d}\theta \\ &= \frac{-k_z \pi L}{8k_s^2} \left[-k_z^2 \chi_1\left(\frac{L}{2}\right) + \frac{1}{2} k_s^2 \chi_1\left(\frac{L}{2}\right) + \frac{1}{2} k_s^2 k_\beta \mathrm{H}_1\left(k_\beta \frac{L}{2}\right)\right];\end{aligned} \tag{A39}$$

$$\begin{aligned}\int_{S_{\mathrm{BE}}} \frac{\partial H_{zz}}{\partial y} \mathrm{d}S_{\mathrm{BE}} &= \int_{S_{\mathrm{SC}}} (\bar{\sigma}_{xz}^{z,y} \cos\theta + \bar{\sigma}_{yz}^{z,y} \sin\theta) \mathrm{d}S_{\mathrm{SC}} - \int_V \rho \frac{\partial \ddot{G}_{zz}}{\partial z} \mathrm{d}V \\ &= \int_0^{\pi} (\bar{\sigma}_{xz}^{z,y} \cos\theta + \bar{\sigma}_{yz}^{z,y} \sin\theta) \frac{L}{2} \mathrm{d}\theta \\ &\quad + \rho\omega^2 \int_0^{\pi}\int_0^{L/2} \frac{\partial G_{zz}}{\partial z} r \mathrm{d}r\, \mathrm{d}\theta = \frac{\mathrm{i}L}{2} \left[\frac{k_\beta^2}{L} \int_0^{L/2} \mathrm{H}_0(k_\beta r) \mathrm{d}r \right. \\ &\quad + \frac{k_z^2}{L} \int_0^{L/2} \mathrm{H}_0(k_\alpha r) \mathrm{d}r + \frac{k_z^2}{k_s^2} \chi_2\left(\frac{L}{2}\right) - \frac{2k_z^2}{Lk_s^2} \chi_1\left(\frac{L}{2}\right) \\ &\quad - \frac{k_\beta^2}{2} \mathrm{H}_2\left(k_\beta \frac{L}{2}\right) + \frac{k_\beta}{L} \mathrm{H}_1\left(k_\beta \frac{L}{2}\right) - \frac{k_\beta^2}{2} \mathrm{H}_0\left(k_\beta \frac{L}{2}\right) \\ &\quad \left. - \frac{k_z^2}{2} \mathrm{H}_0\left(k_\alpha \frac{L}{2}\right)\right].\end{aligned} \tag{A40}$$

The required integrations associated with $\bar{G}_{i1}(\mathbf{x}, n_n, \mathbf{x}_0, \omega)$ are performed in closed form [41,42].

A.2. Hypersingular integrations resulting from Eq. (8), applied in the interior domain (fluid medium)

When the element being integrated is the loaded one, the following integral becomes hypersingular,

$$\begin{aligned}\int_{S_{BE}} \overline{H}_{\mathrm{f}}(\mathbf{x}, n_n, \mathbf{x}_0, \omega) dS_{BE} &= \int_{S_{BE}} \frac{\mathrm{i}}{4} k_{\alpha\mathrm{f}} \left[-k_{\alpha\mathrm{f}} \mathrm{H}_2(k_{\alpha\mathrm{f}} r) \right. \\ &\quad \times \left(\frac{\partial r}{\partial x} \frac{\partial x}{\partial n_n} + \frac{\partial r}{\partial y} \frac{\partial y}{\partial n_n} \right)^2 \\ &\quad \left. + \frac{\mathrm{H}_1(k_{\alpha\mathrm{f}} r)}{r} \right] \mathrm{d}S_{\mathrm{BE}}.\end{aligned} \tag{A41}$$

This integral can be evaluated analytically, using a similar indirect procedure, which is defined by computing the dynamic equilibrium of a semi-cylinder bounded by the boundary element, and leading to:

$$\begin{aligned}\int_{S_{\mathrm{BE}}} \bar{H}_{\mathrm{f}}(\mathbf{x}, n_n, \mathbf{x}_0, \omega) \mathrm{d}S_{\mathrm{BE}} &= \int_0^{\pi} \frac{\mathrm{i}}{4} k_{\alpha_{\mathrm{f}}} \left[-\frac{\mathrm{H}_1(k_{\alpha_{\mathrm{f}}} r)}{r} + k_{\alpha_{\mathrm{f}}} \mathrm{H}_0(k_{\alpha_{\mathrm{f}}} r) \right] \\ &\quad \times \frac{L}{2} \sin\theta \mathrm{d}\theta + \rho\omega^2 \frac{\mathrm{i}}{4} k_{\alpha_{\mathrm{f}}} \\ &\quad \times \int_0^{L/2} \mathrm{H}_1(k_{\alpha_{\mathrm{f}}} r) r \mathrm{d}r \int_0^{\pi} \sin\theta \mathrm{d}\theta \\ &= \frac{i}{2} (k_{\alpha_{\mathrm{f}}})^2 \left[\int_0^{L/2} \mathrm{H}_0(k_{\alpha_{\mathrm{f}}} r) \mathrm{d}r - \frac{1}{k_{\alpha_{\mathrm{f}}}} \mathrm{H}_1\left(k_{\alpha_{\mathrm{f}}} \frac{L}{2}\right) \right].\end{aligned} \tag{A42}$$

The integral $\int_0^{L/2} \mathrm{H}_0(k_{\alpha_{\mathrm{f}}} r) \mathrm{d}r$ is evaluated as:

$$\begin{aligned}\int_0^{L/2} \mathrm{H}_0(k_{\alpha_{\mathrm{f}}} r) \mathrm{d}r &= \frac{L}{2} \mathrm{H}_0\left(k_{\alpha_{\mathrm{f}}} \frac{L}{2}\right) + \pi \frac{L}{4} \left[\mathrm{H}_1\left(k_{\alpha_{\mathrm{f}}} \frac{L}{2}\right) \mathrm{S}_0\left(k_{\alpha_{\mathrm{f}}} \frac{L}{2}\right) \right. \\ &\quad \left. - \mathrm{H}_0\left(k_{\alpha_{\mathrm{f}}} \frac{L}{2}\right) \mathrm{S}_1\left(k_{\alpha_{\mathrm{f}}} \frac{L}{2}\right) \right].\end{aligned} \tag{A43}$$

References

[1] Paillet FL, White JE. Acoustic modes of propagation in the borehole and their relationship to rock properties. Geophysics 1982;47:1215–28.

[2] Baker LJ, Winbow GA. Multipole P-wave logging in formations altered by drilling. Geophysics 1988;53:1207–18.

[3] António J, Tadeu A. The use of monopole and dipole sources in crosswell surveying. J Appl Geophys 2004;56(4):231–45.

[4] Achenbach JD, Lin W, Keer LM. Mathematical modeling of ultrasonic wave scattering by sub-surface cracks. Ultrasonics 1986;24:207–15.

[5] Achenbach JD. Modeling for quantitative non-destructive evaluation. Ultrasonics 2002;40:1–10.

[6] Huang JY. Interaction of SH-waves with a finite crack in a half-space. Eng Fract Mech 1995;51(2):217–24.

[7] Pointer T, Liu E, Hudson JA. Numerical modeling of seismic waves scattered by hydrofractures: application of the indirect boundary element method. Geophys J Int 1998;135:289–303.

[8] Tadeu AJB, Kausel E, Vrettos C. Scattering of waves by subterranean structures via the boundary element method. J Soil Dyn Earthquake Eng 1996;15(6):387–97.

[9] Pao YH, Mow CC. Diffraction of elastic waves and dynamic stress concentrations. New York: Crane-Russak; 1973.

[10] Trifunac MD. Surface motion of a semi-cylindrical alluvial valley for incident plane SH waves. Bull Seismol Soc Am 1971;61:1755–70.

[11] Waas G. Linear two-dimensional analysis of soil dynamics problems in semi-infinite layered media. PhD dissertation. Berkeley, CA: University of California; 1972.

[12] Lysmer J, Udaka T, Seed HB, Hwang R. LUSH—a computer program for complex response analysis of soil-structure systems. Report no. EERC 74-4. Earthquake Engineering Research Center. Berkeley, CA: University of California; 1974.

[13] Stephen RA, Cardo-Casas F, Cheng CH. Finite difference synthetic acoustic logs. Geophysics 1985;50:1588–609.

[14] Leslie HD, Randall CT. Multipole sources in boreholes penetrating anisotropic formations: Numerical and experimental results. J Acoust Soc Am 1992;91:12–27.
[15] Yoon KH. McMechan GA. 3-D finite difference modelling of elastic waves in borehole environments. Geophysics 1992;57:793–804.
[16] Cheng N, Cheng CH, Toksöz MN. Borehole wave propagation in three dimensions. J Acoust Soc Am 1995;97:3483–93.
[17] Ellefsen KJ. Elastic wave propagation along a borehole in an anisotropic medium. PhD thesis. Cambridge, MA: MIT; 1990.
[18] Sinha BK, Norris AN, Chang SK. Borehole flexural modes in anisotropic formations. 61st SEG Annual Meeting Expanded Abstracts, Houston; 1991.
[19] Norris AN, Sinha BK. Weak elastic anisotropy and the tube wave. Geophysics 1983;58:1091–8.
[20] Bouchon M, Schmitt DP. Full wave acoustic logging in an irregular borehole. Geophysics 1989;54:758–65.
[21] Bouchon M. A numerical simulation of the acoustic and elastic wavefields radiated by a source in a fluid-filled borehole embedded in a layered medium. Geophysics 1993;58:475–81.
[22] Dong W, Bouchon M, Toksöz MN. Borehole seismic-source radiation in layered isotropic and anisotropic media: boundary element modelling. Geophysics 1995;60:735–47.
[23] White JE, Sengbush RL. Shear waves from explosive sources. Geophysics 1963;28:1001–19.
[24] Ben-Menahem A, Kostek S. The equivalent force system of a monopole source in a fluid-filled open borehole. Geophysics 1990;56:1477–81.
[25] De Hoop AT, De Hon BP, Kurkjian AL. Calculation of transient tube wave signals in cross-borehole acoustics. J Acoust Soc Am 1994;95: 1773–89.
[26] Cruse TA. Boundary element analysis in computational fracture mechanics. Dordrecht: Kluwer Academic; 1987.
[27] Sládek V, Sládek J. Transient elastodynamics three-dimensional problems in cracked bodies. Appl Math Model 1984;8:2–10.
[28] Sládek V, Sládek J. A boundary integral equation method for dynamic crack problems. Eng Fract Mech 1987;27(3):269–77.
[29] Takakuda K. Diffraction of plane harmonic waves by cracks. Bull JSME 1983;26(214):487–93.
[30] Rudolphi TJ. The use of simple solutions in the regularisation of hypersingular boundary integral equations. Math Compnt Model 1991;15: 269–78.
[31] Lutz E, Ingraffea AR, Gray LJ. Use of 'simple solutions' for boundary integral methods in elasticity and fracture analysis. Int J Numer Methods Eng 1992;35:1737–51.
[32] Watson JO. Hermitian cubic boundary elements for plane problems of fracture mechanics. Int J Struct Methods Mater Sci 1982;4:23–42.
[33] Watson JO. Singular boundary elements for the analysis of cracks in plane strain. Int J Numer Methods Eng 1995;38:2389–411.
[34] Prosper D. Modeling and detection of delaminations in laminated plates. PhD thesis. Cambridge: MIT; 2001.
[35] Prosper D, Kausel E. Wave scattering by cracks in laminated media. In: Atluri SN, Nishioka T, Kikuchi M, editors. Proceedings advances in computational engineering and sciences. Proceedings of the International conference on computational engineering and science ICES'01. Tech Science Press; 2001.
[36] Aliabadi MH. A new generation of boundary element methods in fracture mechanics. Int J Fract 1997;86:91–125.
[37] Chen JT, Hong HK. Review of dual boundary element methods with emphasis on hypersingular integrals and divergent series. Appl Mech Rev 1999;52:17–33.
[38] Aliabadi MH. The boundary element method. Application in solids and structures, vol. 2. London: Wiley; 2002.
[39] Bouchon M, Aki K. Discrete wave-number representation of seismic-source wave field. Bull Seism Soc Am 1977;67:259–77.
[40] Tadeu A, Kausel E. Green's functions for two-and-a-half dimensional elastodynamic problems. J Eng Mech ASCE 2000;126(10):1093–7.
[41] Tadeu A, Santos P, Kausel E. Closed-form integration of singular terms for constant, linear and quadratic boundary elements—part I: SH wave propagation. EABE Eng Anal Bound Elem 1999;23(8):671–81.
[42] Tadeu A, Santos P, Kausel E. Closed-form integration of singular terms for constant, linear and quadratic boundary elements—part II: SV-P wave propagation. EABE Eng Anal Bound Elem 1999;23(9):757–68.
[43] Guiggiani M. Formulation and numerical treatment of boundary integral equations with hypersingular kernels Singular integrals in boundary element methods. Southampton (UK) & Boston (USA): Computational Mechanics Publications; 1998.
[44] Tadeu AJB. Modelling and seismic imaging of buried structures. PhD thesis. Cambridge: MIT; 1992.
[45] Kausel E, Roesset JM. Frequency domain analysis of undamped systems. J Eng Mech ASCE 1992;118(4):721–34.